Ricerca di Sistema elettrico

Relazione finale - Contratto di appalto per attività di sviluppo dei sistemi di alimentazione elettrica dei magneti di JT-60SA Contratto ENEA-RFX del 07/08/2012

Consorzio RFX

CONSORZIO RFX
Ricerca Formazione Innovazione

Report RdS/2013/283

RELAZIONE FINALE – CONTRATTO DI APPALTO PER ATTIVITÀ DI SVILUPPO DEI SISTEMI DI ALIMENTAZIONE ELETTRICA DEI MAGNETI DI JT-60SA CONTRATTO ENEA-RFX DEL 07/08/2012

Consorzio RFX

Settembre 2013

Report Ricerca di Sistema Elettrico

Accordo di Programma Ministero dello Sviluppo Economico - ENEA
Piano Annuale di Realizzazione 2012
Area: Produzione di energia elettrica e protezione dell'ambiente
Progetto: Attività di fisica della fusione complementari a ITER
Obiettivo: *Realizzazione degli "Switching Network Unit" (SNU)*, *Realizzazione di parte degli alimentatori dei magneti poloidali di JT-60SA*
Responsabile del Progetto: Ing. Aldo Pizzuto, ENEA

CONSORZIO RFX
Ricerca Formazione Innovazione

Contratto di appalto per attività di sviluppo dei sistemi di alimentazione elettrica dei magneti di JT-60SA

Contratto ENEA-RFX del 07/08/2012

Relazione finale

EXECUTIVE SUMMARY

With reference to the submitted documents:

- PROCUREMENT ARRANGEMENT FOR THE SUPPLY OF THE SWITCHING NETWORK UNITS FOR CENTRAL SOLENOIDS FOR THE SATELLITE TOKAMAK PROGRAMME
  Annex B – Technical Specifications

- PROCUREMENT ARRANGEMENT FOR THE SUPPLY OF TOROIDAL FIELD, POLOIDAL FIELD AND FAST PLASMA POSITION CONTROL COILS POWER SUPPLIES FOR THE SATELLITE TOKAMAK PROGRAMME
  Annex B – Technical Specifications

the present report collects some specific comments to the technical specifications and studies and analyses performed, relevant to the above mentioned procurement arrangements

INDEX

Comments to the documents:

Procurement arrangement for the supply of the switching network units for central solenoids for the satellite tokamak programme. Annex B – Technical Specifications

Procurement arrangement for the supply of the toroidal field, poloidal field and fast plasma position control coils power supplies for the satellite tokamak programme. Annex B – Technical Specifications

Below some comments common to the technical specifications of both the procurement arrangements STP SNU PA – Annex B and STP SCMPS PA – Annex B.

1 General comments to STP SNU PA and STP SCMPS PA

The technical specifications are well organized and the functional and technical requirements are clearly presented.

The scope of the supply, main deliverables and delivery schedule are clearly stated in the first sections. It is recommended to press so as the list of recommended spare is really delivered before the closing of the detailed design phase.

2 Comments on technical requirements of STP SNU PA and STP SCMPS PA

Specification of the maximum overcurrents

The maximum current value for the SNU is specified equal to ±23 kA (STP SNU PA, Table 4.3-1).

The same value is specified for the crowbar units of the PFC PSs, while the value of the maximum currents in the crowbar units of the FPPCC PSs is equal to 38 kA (STP SCMPS PA, Table 4.2.20-1).

These are very important data and seem specified with sufficient margin on the basis of the results of dedicated analyses performed on this matter.

In fact, the value of the maximum currents have been calculated for transients in the poloidal circuits in case of plasma disruption and Quench Protection Circuit intervention. The overcurrents are due to the mutual coupling among the 10 poloidal superconducting coils, the in- vessel coils, the vacuum vessel, the stabilizing plates and the plasma. In case of rapid variation of current in one of the circuits, overcurrent is induced in the other mutual coupled circuits. To quantify it, a complete model of the poloidal circuits, including all coupled elements have been worked out; the model have been utilized to analyze plasma disruption and Quench Protection Circuit intervention in a large variety of different conditions to calculate the overcurrents and to identify the maximum level. These overcurrents also circulated in the Switching Network and SuperConducting Magnet Power Supply; therefore these analyses are useful for the definition of the functional requirements of the technical specification for all the power supply equipments of the JT-60SA poloidal circuits.

In particular, the maximum currents in the CS coils can reach about 22.5 kA in the worst condition of failure of one Quench Protection circuit in one of the central solenoid coil circuits while the maximum current value in the FPPCC can reach about 35 kA. .

The analyses performed and the relevant results are described and discussed in the attached document N. 1.

Power and control interfaces

The interfaces are clearly described; however, it is suggested to further define them during the detailed design phase; developing as soon as possible detailed drawing of the power terminations, definitions of the pipes, detailed list of interface control signals, hardware front-end and internal control state machine, protection logics and discussing them since the very beginning with JA colleagues.

3 Comments to: “Documentation to be supplied”

The list of the required documentation seems comprehensive; it is recommended to press so as the first draft of all the documents is delivered as soon as possible, since the very beginning, such that there is always the possibility to verify what has been really performed and to have time enough to refine them before the delivery.

Additional specific comments to the document: Procurement arrangement for the supply of the switching network units for central solenoids for the satellite tokamak programme. Annex B – Technical Specifications

4 Comments to STP SNU PA Functional specification and general requirements

Functional parameters (Table 4.3-1)

The SNU operation is defined unidirectional in the text, but in the table 4.3-1 the current specification is ±20 kA. If the current reverse will be effectively performed via current reversing links and the current in SNU will be always unidirectional, it is suggested to clarify this apparent inconsistency.

5 Comments to STP SNU PA – "Reference scheme and related main components technical requirements"

Reference scheme – IGCTs turn-on behaviour

The reference design suggested in the Annex B to realize the desired current commutation from the closed switch to the resistor at the plasma breakdown, consists in a hybrid circuit breaker composed of a mechanical switch and a static one in parallel, based on Integrated Gate Commutated Thyristors (IGCTs).

This solution was also suggested in the Technical Specifications of the Quench Protection Circuits and then realized; such that we can confirm its feasibility.

Nevertheless, a significant amount of technical issues have been analyzed in the past years at Consorzio RFX before reaching the feasibility confidence.

One of the main issues faced first, before confirming the hybrid mechanical-static scheme, was the verification of reliable turn-on of many IGCTs in parallel with very low voltage applied between anode and cathode; in fact, in this hybrid configuration the static switch is turned-on by the arc voltage of the mechanical switch, which is quite low. The previous experience with thyristors, in particular those commanded via optic fibers, was that at least 100 V are necessary between another and cathode to assure a safe turn-on. This is not the case

of the present application in JT-60SA, where the arc voltage of a mechanical bypass switch in air can be less than 30 V.

The ABB company was confident on a different operation of the IGCTs with respect to thyristors, but was not available to give guarantees on the minimum voltage for a safe turn-on, due to lack of real applications of that operating conditions.

For these reasons specific tests have been designed, a dedicated circuit set up, and a test campaign performed to gain direct confidence on the turn-on behaviour of the IGCTs. The main results and relevant discussion are described in the attached document N. 2; they proved that a safe turn-on can be guaranteed with very low voltage, of the order of few volts.

Reference scheme – current commutation between BPS and static CB

Also the verification that the current commutation between BPS and static CB can be sufficiently fast and reliable was a key issue which we can today consider proved.

The encouraging results obtained with the IGCTs turn-on tests were not sufficient to confirm that this hybrid topology was well adequate to interrupt tens of kilo-ampere; in fact, the correct operation of the Hybrid CB requires that the voltage of the arc current, appearing at the BPS terminals when it starts opening, is able not only to turn-on the IGCTs connected in parallel, but also to quickly drive the complete current commutation from the BPS to the static devices. The characterization of the commutation process was analyzed in detail to assure the hybrid CB reliability.

In addition, another key aspect to be explored was the knowledge of the BPS arc voltage behavior at different current values, which investigation definitely required experimental tests.

For these reasons a 10 kA prototype of hybrid CB was developed, whose operation permitted to gain experience on the current commutation from the BPS to the static CB at a significant current level and to assess the reliability of such technical solution. The tests performed and relevant results are described in the attached document N. 3.

6 Comments to STP SNU PA – “Testing and approval requirement”

The set of type and routine tests specified seems adequate to assure a full verification of the system design and performance.

Type tests are extremely important to check the suitability of the design and to prove the performance, therefore it is recommended to take particular care about them.

As for the Quench Protection Circuit procurement, a significant part of the type tests have been performed at Consorzio RFX. A dedicated circuit has been designed and set-up, which is described in the attached document N. 4; moreover, a circuit description with the aim to verify electromagnetic risk of the tests to fulfill the foreseen safety requirement for their execution is given in the attached document N. 5. These documents can be useful as a reference for the future test circuit to perform the type tests of the Switching Network.

Additional specific comments to the document: Procurement arrangement for the supply of the switching network units for central solenoids for the satellite tokamak programme. Annex B – Technical Specifications

1 Comments to STP SCMPS PA – "Technical requirements"

Fault conditions and protective actions

The specifications correctly indicate that the converter is able to perform the suitable protective actions in case of all the fault conditions.

It is suggested to discuss in details this topic during the DDP and asking the Supplier to describe in detail the analyses performed to simulate the faults and demonstrate the suitability of the design and effectiveness of the protection action.

For TFC, CS2 and CS3 PSs, for which the relevant transformers is included in the procurement too, it could be of interest the analyses of the short circuit currents in case of a fault at the connection point between the ac cables and the thyristor bridge of the converters. A description of these analyses for the specific case of TFC PS is given in the attached document N. 6.

Operational requirements for PFC PS units

The specified typical operational pulse sequence (section 4.4.3) foresees that all the ac HV circuit breakers and disconnectors are in the open state before a plasma pulse, that they are closed just before premagnetization and that they are opened again after the pulse completion. Certainly, the operational requirement and the impact of the finite state machine which will be designed to control the convert operation will be discussed in detail during the DDP, but it is suggested to consider the opportunity to avoid opening all the circuit breaker every plasma pulse unless a fault condition do not command their opening.

Redundancy and safety factor (section 4.2.2)

The current sharing factor in case of components connected in parallel is indicated greater or equal to 1.2; probably it should have been indicated lower or equal to 1.2.

Attachment 1.

EXCERPT FROM CONSORZIO RFX INTERNAL NOTE: RFX_BA_TN_08:

Plasma disruption and quench protection in JT-60SA poloidal circuits

1 Introduction

The new satellite tokamak JT-60SA will be equipped with a number of magnets aimed at producing the magnetic fields for the generation and position control of the plasma current. Both superconducting and copper magnets will be installed. The toroidal circuit is composed of 18 superconducting magnets rated for 25.7 kA steady state current. The poloidal circuits are composed of 10 superconducting magnets, including 4 Central Solenoid (CS) and 6 Equilibrium Field (EF) coils, rated for 20 kA with a duty cycle of 100 s every 30 minutes and 2 copper Hybrid Control (HC) in-vessel coils rated for 5 kA. A sketch of the machine cross section is shown in Figure 2.1.

As shown in Figure 2.2, all the toroidal magnets are connected in series and are supplied by a single low voltage Power Supply (PS). Instead, the poloidal superconductors are inserted in ten separated circuits as shown in Figure 2.3 and Figure 2.4, each one independently fed by a dedicated power supply. Some of the poloidal circuits are also equipped with booster converter or switching network to aid plasma breakdown.

In case of loss of the coil superconducting status (quench) or in case of faults requiring a fast discharge of the magnets, the energy stored in the superconducting magnets has to be rapidly removed by means of Quench Protection Circuits (QPC). For this reason a QPC is connected in each circuit including a superconducting coil, and it is composed of a dc circuit breaker paralleled to a dump resistor, as showed in Figure 2.5. In normal operation the dc circuit breaker is closed and the coil current flows through it; in case of quench or in case of other severe circuit faults the dc circuit breaker is opened and the dump resistor is inserted in the coil circuit, permitting the rapid current discharge. An explosive activated fuse (pyrobreaker) is inserted in series to the circuit breaker and is operated as a backup protection in case of dc circuit breaker failure.

The characteristics of the QPCs as resulting from the superconducting magnets requirements are shown in Table 2.1. However, the actual rating of the QPCs depends on the maximum current that under different situations can flow in the coils. In the toroidal circuit no significant over-current is expected, even in case of the faults analyzed in this work, because all toroidal coils are connected in series and they have no significant magnetic coupling with other conductors.

On the contrary the poloidal circuit is quite complex, due to the mutual coupling among the 10 poloidal superconducting magnets, the two Hybrid Control (HC) in-vessel coils, the vacuum vessel,

the stabilizing plates and the plasma. In case of rapid variation of current in one of the circuits, overcurrent is induced in other mutual coupled circuits. Thus, the maximum current that the poloidal QPCs must interrupt could exceed the coil nominal current, and the assessment of such value requires a detailed analysis of the operation of the JT-60SA poloidal circuits with a complete model including all coupled elements.

The utility of working-out the poloidal circuit complete model is not only limited to the evaluation of the QPC maximum current, but it can be exploited for more general and global analyses. In fact the complexity of the poloidal circuits requires for taking into account all the mutual coupled elements to correctly reproduce their actual current waveforms both in normal and anomalous conditions. This means that the definition of the detailed specifications for the poloidal components and their optimization can be derived only by means of analyses performed using the complete model. Part of these studies have been published in Ref. [14].

Table 2.1 – ***QPC characteristics as resulting from superconductor requirements***

Characteristic	**Toroidal QPC**	**Poloidal QPC**
Unit number	3	10
Nominal voltage	2.8 [kV]	< 5 [kV]
Nominal current	25.7 [kA]	20 [kA]
Current polarity	Unidirectional	Bidirectional
Duty cycle	Steady state	100 s / 30 min
Maximum allowed I^2t	5.3 [GA^2s]	2 [GA^2s]
Maximum delay from command	1 [s]	1 [s]
Maximum delay for pyrobreaker operation	1 [s]	1 [s]
Maximum time to restart after intervention	60 [minutes]	30 [minutes]

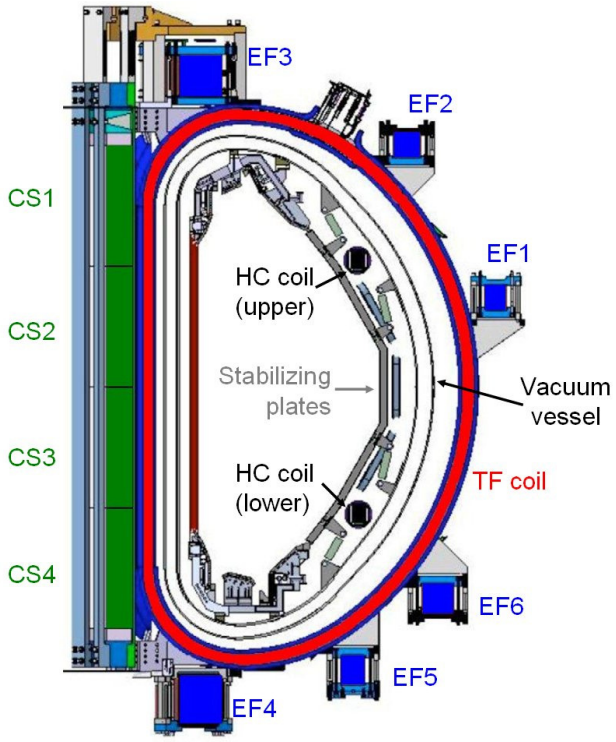

Figure 2.1 – *Poloidal cross section of JT-60SA*

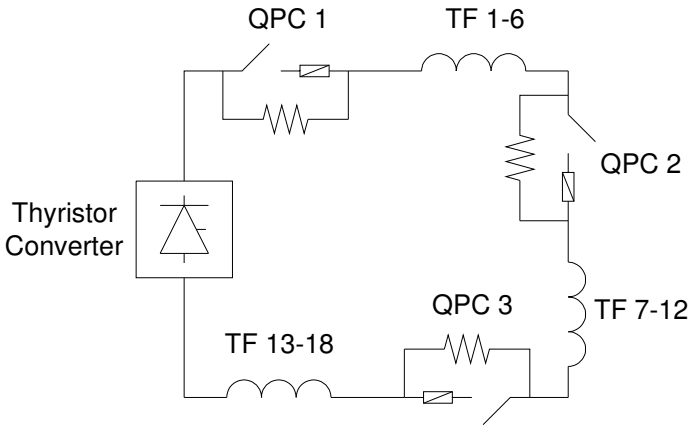

Figure 2.2 – ***Toroidal*** *Circuit*

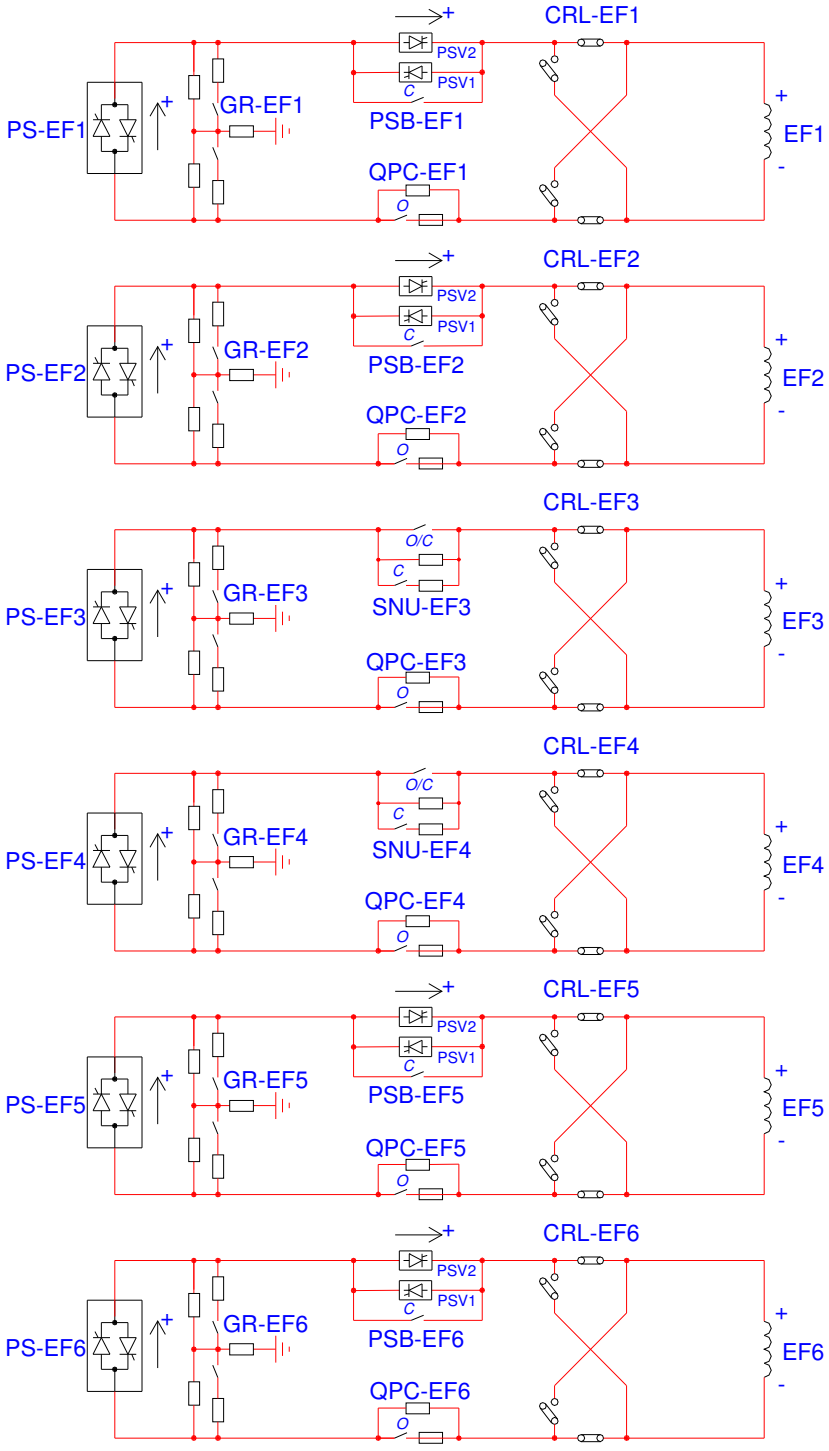

Figure 2.3 – EF Circuits

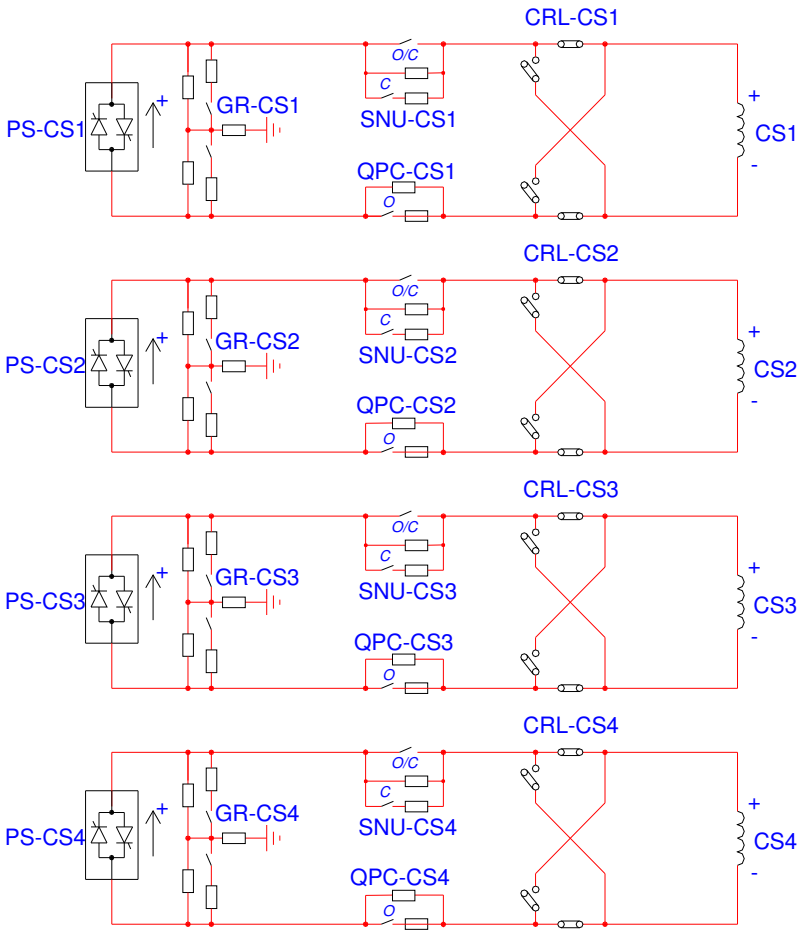

Figure 2.4 – CS Circuits

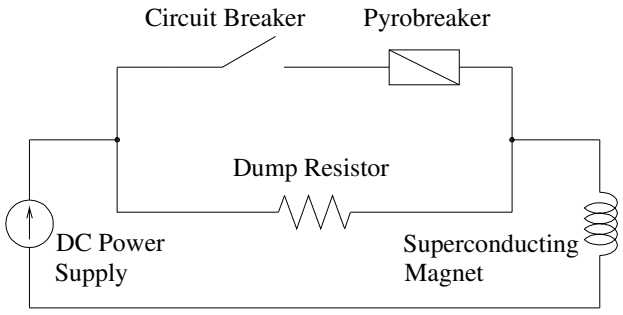

Figure 2.5 - Conceptual scheme of the Quench Protection Circuit

2 JT-60SA Poloidal Circuit Model

A detailed axial-symmetric layout of all the poloidal conductors has been worked out as a first step, taking into account the dimensions of each element of the poloidal circuits at its operating temperature. The turn numbers, dimensions and positions of superconducting coils at the operating temperature of 4 K are shown in Table 2.2. In this table R and Z represent the horizontal and vertical coordinates, respectively, of the magnet central position in the axial symmetric coordinate system; ΔR and ΔZ are the horizontal and vertical sizes of the magnets.

Table 2.2 – Coil geometrical characteristics

Coil	Turn number	R (mm) @4K	Z (mm) @4K	ΔR (mm) @4K	ΔZ (mm) @4K
CS1	556	821.93	2386.5	327	1560.4
CS2	556	821.93	795.51	327	1560.4
CS3	556	821.93	-795.5	327	1560.4
CS4	556	821.93	-2387	327	1560.4
EF1	142	5801.3	1178.7	329.3	333.8
EF2	154	4607.1	3170.5	356.7	333.8
EF3	248	1913.1	4025	542.2	427.3
EF4	355	1913.1	-4117	542.2	610.8
EF5	152	3902.4	-3722	301.9	389.6
EF6	180	5039.2	-2774	356.7	389.6
HC in-vessel upper	16	4045	1665	148	204
HC in-vessel lower	16	4045	-1665	148	204

As a second step each element has been discretized with a sufficient number of circular conductors, named filaments, to achieve a good approximation. For the CS and EF coils, the number

of filaments, their position and their radius have been selected so as to precisely mimic the number and the geometrical characteristics of the conductors composing the coils. For the HC coils the number of filaments used for the mutual inductance matrix calculation is higher than the coil turn number; in order to have a more detailed discretization, a number of filaments six times the turn number has been used, and their radius has been calculated so as to completely cover the HC coil cross section area.

The JT-60SA vacuum vessel is torus-shaped and double-walled. The double-wall cavity is filled with borated water to enhance the neutron shielding capability of the vacuum vessel. Every 40 degree, the vessel is attached at the bottom to a gravity support with a pack of spring plates. In the model the vacuum vessel has been discretized with 154 conductors, placed in a central position in respect with the vessel inner and outer walls.

To improve plasma stabilization, stabilizing plates have been designed as a double-wall structure placed inside the vessel, and are covered with bolted carbon armour tiles on cooled heatsinks as a first wall. Similarly to the vessel, the stabilizing plates have been discretized with 36 conductors placed in a central position in respect with their inner and outer walls. The size, the position and the number of filaments discretizing vessel and stabilizing plates have been selected so that the diameter of each conductor is about the thickness of the vessel and stabilizing plates themselves and so that each filament results consecutive to the other. This thick discretization permits to reproduce with a suitable approximation the different current distributions that could arise during the disruption, in particular in the passive elements close to plasma.

Three principal parameters contribute to the definition of equilibrium plasma current distribution: plasma self inductance l_P which characterizes the stiffness of plasma current profile, normalized plasma beta β_N which accounts for thermal energy content of plasma and the poloidal flux ψ_C linking the plasma geometric center which determines the Ohmic distribution of current in poloidal magnets.

Table 2.3 – Position and current of plasma filaments

Conductor number	**R [mm]**	**Z [mm]**	**Current [MA]**
1	3444.3	676.19	1.45
2	2720.4	1232.8	0.308
3	2493.5	676.19	0.605
4	2504.1	-395.68	0.574
5	2793.9	-910.95	0.502
6	3475.2	-395.68	2.040

As a first step the plasma has been discretized with six conductors, placed in a position and with a current distribution (see Table 2.3) so as to obtain a magnetic field similar to the one produced by a reference 5.5 MA plasma with $l_P = 4.60$ μH, $\beta_N = 1.2296$ and $\psi_C = 16.4$ Wb. Other more refined plasma discretizations will be discussed in paragraph 3.3. A sketch of the obtained model is showed in Figure 2.6.

Figure 2.6 - Geometrical model of the poloidal circuits of JT-60SA

2.1 Mutual inductance matrix

For each filament conductor the self inductance value L_i has been calculated as:

$$L_i = 4\pi \cdot 10^{-7} \cdot r_i \cdot \left[\ln\left(\frac{8 \cdot r_i}{R}\right) - 1.75 \right] \qquad (2.1)$$

where r_i is the filament major radius and R is the filament thickness.

The mutual inductance value $m_{i,j}$ of each couple of filaments used to model the coil and the passive elements of JT-60SA has been calculated according to Ref. [15]:

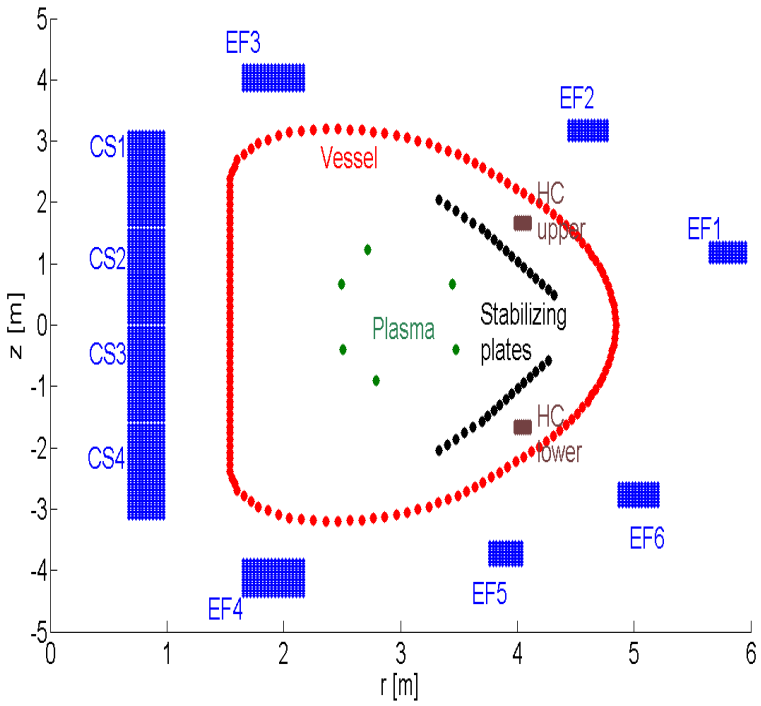

$$m_{i,j} = \frac{8\pi \cdot 10^{-7}}{k} \cdot \sqrt{r_i \cdot r_j} \cdot \left[\left(1 - \frac{k^2}{2} \right) \cdot J_1(k) - J_2(k) \right] \tag{2.2}$$

where:

$$J_1 = \sum_{p=0}^{4} A_p \cdot \left(1 - k^2\right)^p + \ln\left(\frac{1}{1-k^2} \right) \cdot \sum_{p=0}^{4} B_p \cdot \left(1 - k^2\right)^p ,$$

$$J_2 = \sum_{p=0}^{4} C_p \cdot \left(1 - k^2\right)^p + \ln\left(\frac{1}{1-k^2} \right) \cdot \sum_{p=0}^{4} D_p \cdot \left(1 - k^2\right)^p ,$$

$$\mathrm{A} = \begin{pmatrix} 1.38629436112 \\ 0.09666344259 \\ 0.03590092383 \\ 0.03742563713 \\ 0.01451196212 \end{pmatrix} \quad \mathrm{B} = \begin{pmatrix} 0.5 \\ 0.12498593597 \\ 0.06880248576 \\ 0.03328355346 \\ 0.00441787012 \end{pmatrix} \quad \mathrm{C} = \begin{pmatrix} 1 \\ 0.44325141463 \\ 0.06260601220 \\ 0.04757383546 \\ 0.01736506451 \end{pmatrix} \quad \mathrm{D} = \begin{pmatrix} 0 \\ 0.24998368310 \\ 0.09200180037 \\ 0.04069697526 \\ 0.00526449639 \end{pmatrix}$$

In order to find out a single value of self-inductance for each poloidal coil, the mutual inductance values of each single conductor composing each coil have been summed, since the current is the same in the series connected filaments. For vacuum vessel, stabilizing plates and plasma, the contributions of each single filament have been considered separately, in order to easily take into account the possible different current distributions. The resulting inductance matrix size is 207×207.

For vacuum vessel and stabilizing plates the equivalent resistance value of each filament has been calculated supposing that they are connected in parallel and subdividing the total resistance of the conductor proportionally to the length of the filament itself. For the coils it has been considered the total resistance value that is zero for CS and EF superconducting coils and 5.7 mΩ for HC coils.

The mutual inductance matrix and the resistance values have been inserted into a linear system representing the relation between current and voltage of each coil and filament:

$$\begin{cases} V_{Ci} = L_{Ci} \cdot \dfrac{di_{Ci}}{dt} + M_{CiVj} \cdot \dfrac{di_{Vj}}{dt} + M_{CiPk} \cdot \dfrac{di_{Pk}}{dt} \\ V_{Vj} = M_{CiVj} \cdot \dfrac{di_{Ci}}{dt} + L_{Vj} \cdot \dfrac{di_{Vj}}{dt} + M_{VjPk} \cdot \dfrac{di_{Pk}}{dt} + R_{Vj} \cdot i_{Vj} \end{cases} \tag{2.3}$$

where i_{Ci}, i_{Vj}, i_{Pk} are, respectively, the currents in the i-th coil, in the j-th conductor discretizing vessel or stabilizing plates and in the k-th element discretizing plasma; V_{Ci} are the voltages applied to the coils and V_{Vj} are the vessel/stabilizing plates voltages that have assumed as zero since they are short-circuited passive elements; L_{Ci} and L_{Vj} are the coil and vessel/stabilizing plates self-inductances; M_{CiVj}, M_{CiPk} and M_{VjPk} are the mutual inductances between coils, vessel and plasma, and

R_{Vj} are the vessel resistances. Unknown terms are the currents in the coils and in the passive conductors, while the plasma current evolution is imposed. The coil voltage is applied externally, so as to have the possibility of simulating the converter applied voltage. In the model converters are considered as current controlled ideal voltage generators.

The solution of the described linear system permits to obtain the current waveforms in the poloidal circuits in different operating conditions. In particular the cases of plasma disruption and quench protection circuit operation have been widely analyzed. These results have been particularly useful for defining the maximum current in the coils, that is the maximum current value that the QPCs shall interrupt.

3 Plasma Disruption Simulation

Due to the strong mutual coupling, a plasma disruption could cause a significant current variation in the passive elements and in the poloidal coils. In such a situation, it is not easy to identify which are the parameters that have a real impact on the level of induced over-currents on the external coils, so a set of simulations has been performed using the developed model and changing the plasma disruption parameters such as plasma initial current value, plasma position, plasma current distribution and derivative.

During plasma disruption the converters feeding the CS and EF coils can contribute to limit the coil over-current, but it is possible that in some fault conditions they are by-passed. In order to take into account this realistic worst case in the performed simulations, the converters have been considered supplying zero voltage.

Since Eq. (2.3) represents a linear system, the maximum overcurrent in the coils occurs at the maximum plasma current; therefore the case of 5.5 MA was considered in the simulation.

Table 2.4 – ***Coil over-currents in case of fixed position 6 filaments plasma disruption***

3.1 Fixed position, 10ms plasma disruption

In the first case studied the six plasma filaments were kept fixed in the initial position during the disruption with the current in the filaments linearly decreasing from the initial value to zero in 10 ms.

Because of the analytical form of Eq. (2.3), the initial current value of the external superconducting coils at the time of plasma disruption has no effect on the induced coil over-current.

In fact the linear system described by Eq. (2.3) can be written in the following form:

$$\frac{\partial i(t)}{\partial t} = -M^{-1} \cdot R \cdot i(t) + M^{-1} \cdot v(t) \qquad (2.4)$$

whose solution is

$$i(t) = e^{-M^{-1} \cdot R(t-t_0)} \cdot i_0 + \int_{t_0}^{t} e^{-M^{-1} \cdot R(t-t_0)} M^{-1} v(z) \partial z \qquad (2.5)$$

It results that the initial current values i_0 are multiplied by the matrix function $e^{-M^{-1} \cdot R(t-t_0)}$. Since the resistance of superconductive coils is zero, the free evolution of the system with superconductive coils depends only on the initial current on passive conductors having a non zero resistance.

The current on the passive structures at the time of plasma disruption can be considered as zero, since they have very short resistive time constants (in the order of tens of milliseconds) if compared to the foreseen plasma current ramp-up and flat-top duration (in the order of seconds). For these reasons the initial current of coils and passive elements has been set to zero.

The obtained results in terms of over-current are shown in Figure 2.7 and Table 2.4. The maximum EF and CS coil over-current appears in coil CS2, exceeding 3 kA. A large over-current is present in HC in-vessel coils, up to about 35 kA for the upper coil and 27 kA for the lower one, that

Coil	Over-current [kA]	Coil	Over-current [kA]
CS1	1.44	EF3	1.09
CS2	3.07	EF4	0.42
CS3	2.32	EF5	1.10
CS4	0.85	EF6	1.59
EF1	2.77	HC-upper	34.87
EF2	2.17	HC-lower	26.71

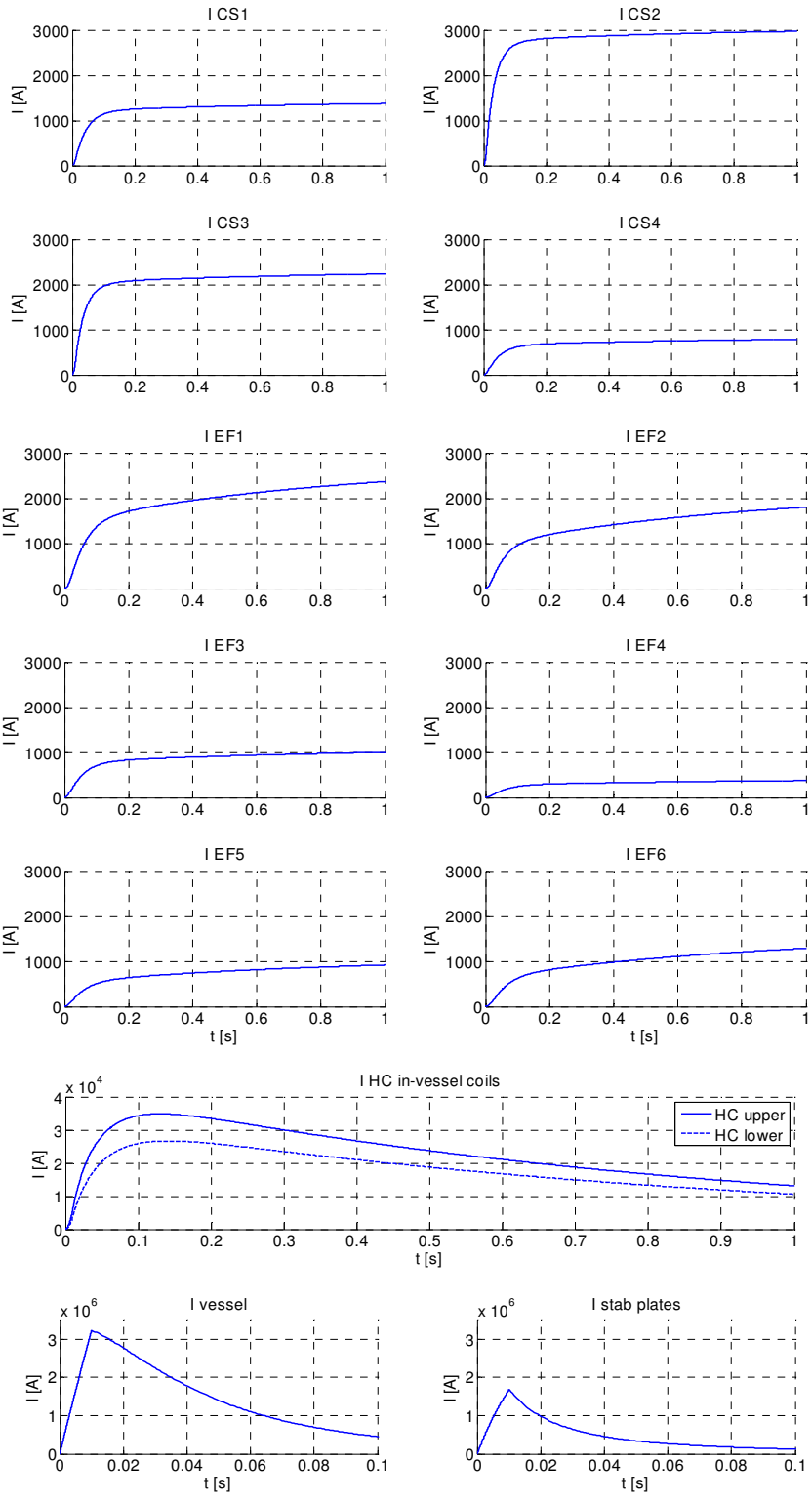

are rated for a nominal current of 5 kA.

Figure 2.7 - Overcurrents in case of plasma disruption obtained with the simplified linear model. Note the different time-scales of bottom panels

3.2 Different plasma current derivative during disruption

As a second step, the plasma disruption has been simulated changing the plasma current derivative value, ranging from 5.5 MA / 1 ms to 5.5 MA / 100 ms. The obtained current waveforms in the external coils, two of which are shown as an example in the first two panels of Figure 2.8, are different only in the initial transient, but the regime over-current value is the same for each considered plasma derivative value, meaning that this disruption parameter has no influence on the level of induced over-current. It is possible to notice that, instead, the vessel induced current waveforms are heavily influenced by the plasma current derivative during disruption.

3.3 Plasma Current Distribution

The aforementioned analyses were made assuming a simple plasma model, composed of six filaments reproducing the magnetic field of reference plasma with a current of 5.5 MA. A more refined reference plasma model, composed of more than 3000 current filaments but with the same β_p and l_P reference values, has been used with the aim of evaluating the effect of the plasma discretization on the resulting external coil overcurrent. The results for the external superconducting magnets, shown in the third column of Table 2.5, do not wander more than 2% of the nominal current in respect to the ones obtained with the six filament model. It is therefore clear that the effect of realistic current profile is negligible for this study. On the contrary a significant difference is obtained in the HC coils, due to the fact that these are internal coils and are more affected by plasma current variation than external ones, since they are not shielded by the presence of low resistance vessel.

Table 2.5 – ***Coil over-currents in case of plasma disruption with different plasma models***

Coil	**Coil overcurrent**			
	6 filaments	**Reference**	**Increased flux**	**Increased l_P**
CS1	1.44	1.15	1.16	1.12
CS2	3.07	2.70	2.69	2.71
CS3	2.32	2.57	2.56	2.59
CS4	0.85	1.02	1.03	1.00
EF1	2.77	3.07	3.11	3.20
EF2	2.17	2.07	2.09	2.11
EF3	1.09	0.92	0.94	0.92
EF4	0.42	0.50	0.51	0.50
EF5	1.10	1.32	1.34	1.34
EF6	1.59	1.91	1.93	1.96
HC-upper	34.87	34.21	34.37	34.89
HC-lower	26.71	32.96	33.0	33.54

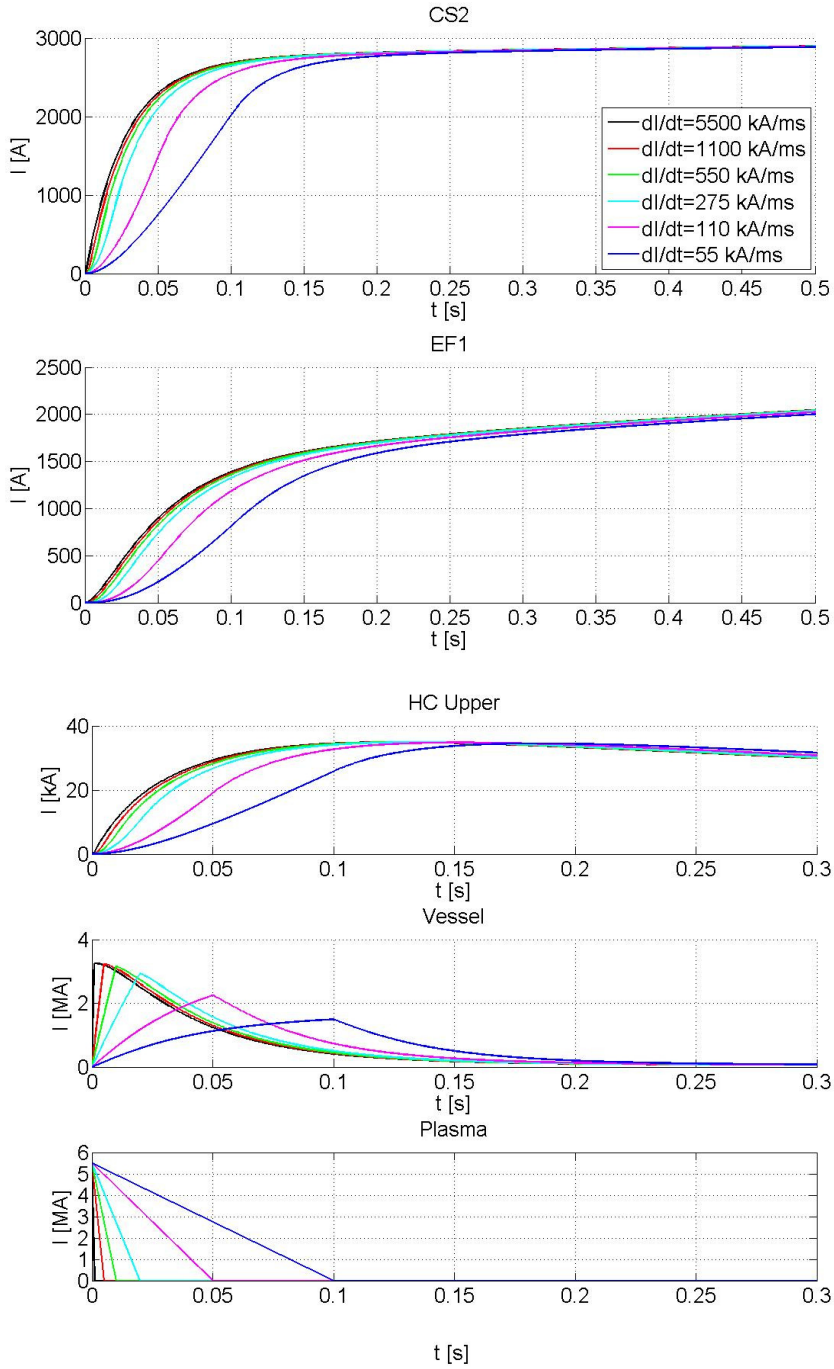

Figure 2.8 – Overcurrents in coils CS2 and EF1, in Upper HC in-vessel coil and in Vessel in case of different plasma current derivative during plasma disruption

A different initial magnetic field created by a different plasma current distribution at the time of disruption could lead to variations of the over-current values both in the HC in-vessel coils and in the superconducting coils, being changed the mutual coupling between coils and plasma. In order to investigate this possibility, a number of plasma scenarios has been considered among the possible plasma equilibrium conditions with 5.5 MA current.

Several equilibrium plasma current distributions have been simulated with the TOSCA code [16] considering different possible combinations of l_P, β_N and ψ_C, obtaining precise plasma current distributions with more than 3000 current filaments. The resulting detailed plasma models have been inserted in the zero-dimensional poloidal circuit model for simulating a disruption with plasma in a fixed position.

The results, reported in columns 4 and 5 of Table 2.5 for two plasma equilibria characterized respectively by an increase in flux consumption ($l_P = 4.6$ μH, $\beta_N = 1.23$ and $\psi_C = 21.4$ Wb) and an increase of l_P ($l_P = 5.06$ μH, $\beta_N = 1.35$ and $\psi_C = 18.8$ Wb) respect with the reference equilibrium, show that with the considered initial plasma current distributions only negligible variations are observed both in superconducting and in-vessel coil overcurrents, meaning that the variation of plasma parameters as flux consumption and l_P has negligible effect on coil overcurrent.

3.4 Plasma Vertical Displacement Event (VDE)

Finally, the effect of plasma movement during a disruption has been studied. In fact it is possible that the combined effect of current derivative and plasma movement could result in a higher overcurrent in the coils where the linked flux is diminishing.

The study of plasma VDE is a specific topic generally faced during the detailed mechanical design of passive structures such as vacuum vessel and stabilizing plates, since it represents one of the worst case conditions for such elements from the point of view of electro-mechanical stresses. The evaluation of the evolution of the plasma column position in case of a VDE is a complex task and it is generally worked out by means of specific plasma equilibrium codes. The VDE calculations performed by the JT-60SA work group for defining the mechanical stresses of in-vessel components with the DINA code [17] have been used as input for obtaining the time evolutions of some plasma current distributions in case of VDE.

The plasma column time evolution in terms of position and current has been fitted in a fixed grid covering all the in-vessel area, each point being a plasma filament. The current in each filament is changed in time so as to reproduce the plasma VDE. In this way it has been possible to reproduce the plasma VDE evolution using the plasma filament discretization inside the simplified linear model.

The results obtained in case of both upward and downward VDEs, as shown in Figure 2.9 for the two coils where the VDE effect is more remarkable, prove that the plasma movement in case of

disruption determines the transient waveform of the current in the external coils, but has no influence on the coil over-current final value.

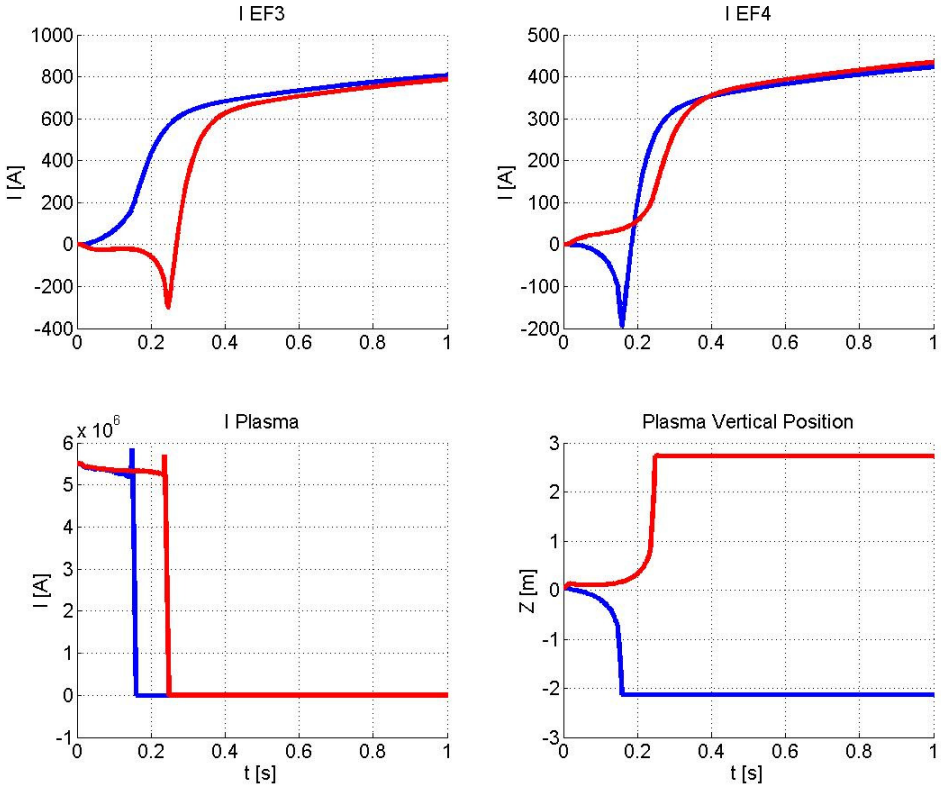

Figure 2.9 – Overcurrents in coils EF3 and EF4 in case of Vertical Displacement Event (upward movement in red, downward movement in blue)

It is interesting to notice that, as expected, the current in the coils where the plasma is approaching starts to become negative while it becomes positive in the coils where the plasma is departing from.

Moreover it is possible to assess that during the transient phase the coil over-current does not reach values higher than the final over-current. This assures that the VDE event is not cause of over-current higher than the ones obtained in a standard plasma disruption.

3.5 Maximum coil overcurrent in case of plasma disruption

Since the variation of plasma parameters as current derivative, current distribution and movement does not have a significant influence on the superconducting coil overcurrent, for finding out the maximum peak current value in one coil in case of plasma disruption, it is sufficient to take into consideration the maximum of the values shown in Table 2.5 for that coil, and to sum this value to the initial coil current value.

If the nominal coil current of 20 kA is considered as initial value, an unacceptable over-current value of more than 15% would be obtained for CS2 and EF1 coils, but this could lead to not realistic conditions: for example the current in CS coils reaches the maximum rated value only before plasma breakdown, while when plasma current reaches 5.5 MA the current in CS coils has lower values. In order to take into consideration more actual initial coil current values, more than 300 realistic sets of coil current values, called snapshots, obtained from plasma equilibrium scan, have been considered.

Considering these snapshots, it results that in case of plasma disruption the higher coil current value is obtained in coil EF4, where the initial current at the time of plasma disruption is 19.95 kA and the final value is 20.46 kA. If other snapshots were proposed, with higher initial current in coils such as EF1 and EF2 where the plasma disruption causes higher over-currents, there would be the possibility of largely exceeding the coil nominal current value of 20 kA.

3.6 Model Validation with Comsol Multiphysics

A simplified axial-symmetric two-dimensional model of the poloidal circuits of JT-60SA has been developed using Comsol Multiphysics [18], a finite element analysis, solver and simulation software package. In the Comsol Multiphysics model the coils have been modeled as single turn massive conductors instead of being composed of a number of series connected conductors; the vessel and the stabilizing plates as continuous conductors and the plasma as 6 conductors as described in previous Section. Plasma disruption has been simulated using this Comsol Multiphysics model and the resulting coil current waveforms have been compared with the ones obtained with the linear system described in previous paragraphs, finding a good agreement as shown in Figure 2.10.

The comparison of the results obtained with the linear system and Comsol Multiphysics can be considered an effective way of validation, since the first is based on analytical calculation, while the latter is based on finite element model analyses involving magnetic field reconstruction.

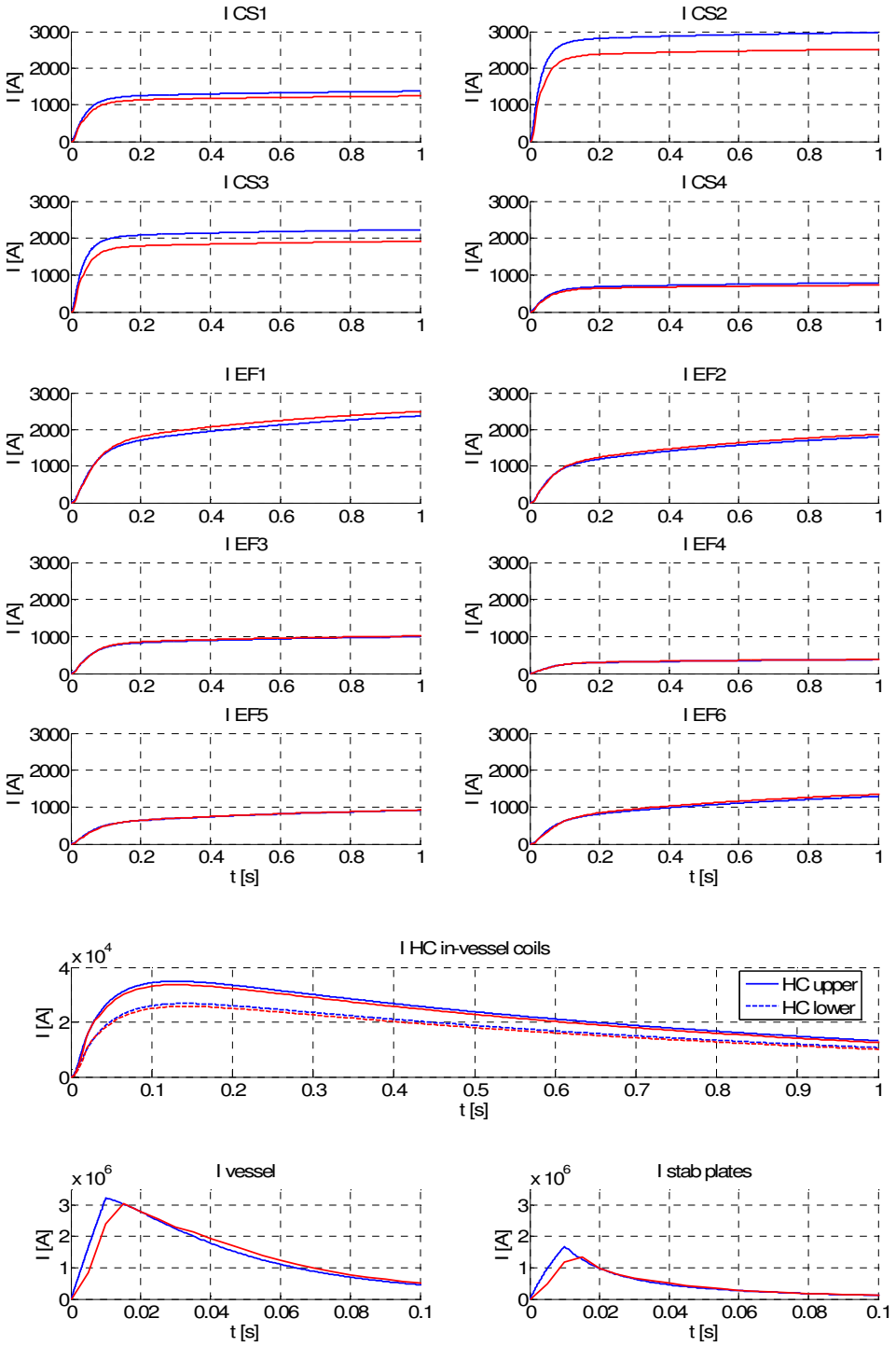

Figure 2.10 - Overcurrents in case of plasma disruption obtained with the simplified linear model (in blue) and with Comsol model (in red). Note the different time-scales of the bottom two panels

4 QPC Intervention Simulation

4.1 Intervention of a single QPC

In case of quench in one superconducting coil it is necessary to activate its QPC to rapidly zero the coil current. By means of the QPC activation, in fact, the dump resistor is inserted in the coil circuit and the current is zeroed with the time constant resulting not only from the R/L of the circuit but also from the mutual inductance with other poloidal circuits. For this reason, to analyze the operation of the QPC it is important to take into consideration the current variations in all coupled circuits and the developed model is a useful tool allowing to perform these studies.

The protection strategy presently adopted foresees that the QPCs are commanded not only in case of quench, but also in case of other faults in the circuits, to fast de-energize the coils; when the QPCs are commanded, all the converters are switched-off and bypassed by crow-bars.

All the QPC are operated in case of quench, while, in case of other faults, it could be acceptable in principle to command the intervention of the QPC in one circuit only. Due to the mutual coupling between coils, it is possible that the current variation in the coil where a single QPC is operated induces overcurrent in other coils.

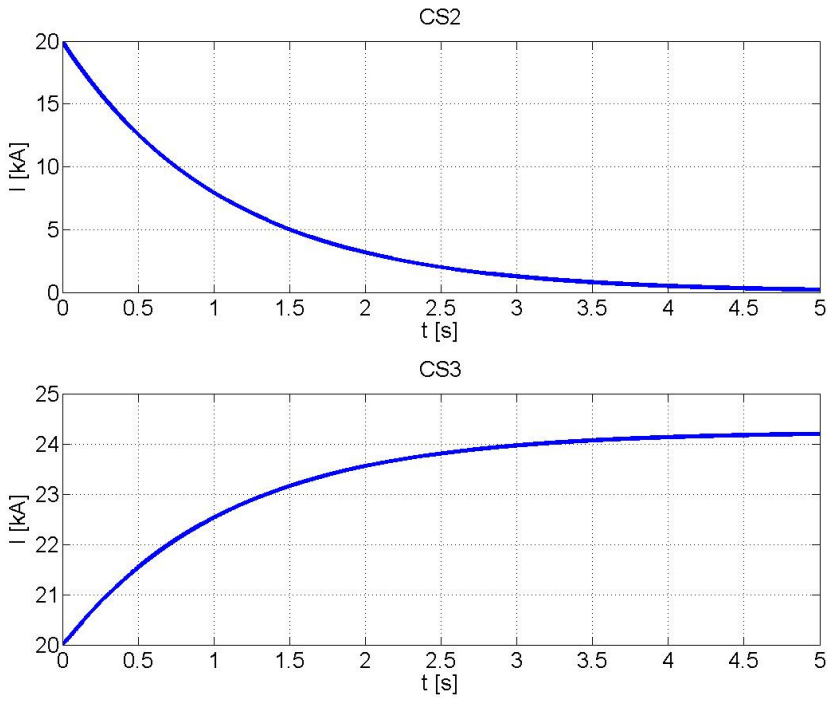

Figure 2.11 – Overcurrent in CS3 coil in case of QPC intervention in coil CS2

In order to study this case, the linear model has been used assuming that the QPC is operated in one coil circuit only, and all the converters are bypassed. In fact this condition represents the worst case in terms of maximum overcurrent, since the action of converters could help in limiting the coil

overcurrent. With this kind of simulations it has been verified that the intervention of a single QPC could lead to excessive current variations in other coils, due to the mutual coupling among them.

A number of possible coil currents initial values have been considered, and the worst case has been found for CS coils: as shown in Figure 2.11, in case of operation of CS2 QPC, the current in CS3 coil can reach more than 24 kA, exceeding by far the coil nominal current. Such value would be too large to be tolerated by the coils; therefore it has been decided as protection strategy to activate always simultaneously all the poloidal QPCs.

4.2 QPC dc circuit breaker failure

In case of failure of the QPC dc circuit breaker, it is necessary to activate the backup pyrobreaker installed in series to the circuit breaker, so as to commutate the current into the discharge resistance. The maximum time between the QPC intervention request and the pyrobreaker activation is 2 s (see Table 2.1). In the time between the QPC activation request and the pyrobreaker activation, the current in the faulty circuit increases due to the mutual coupling with the other poloidal circuits where the current is decreasing. In this case it is necessary to evaluate the maximum current value reached in the faulty QPC.

Thus, for each QPC it has been simulated the case of dc circuit breaker failure starting with a

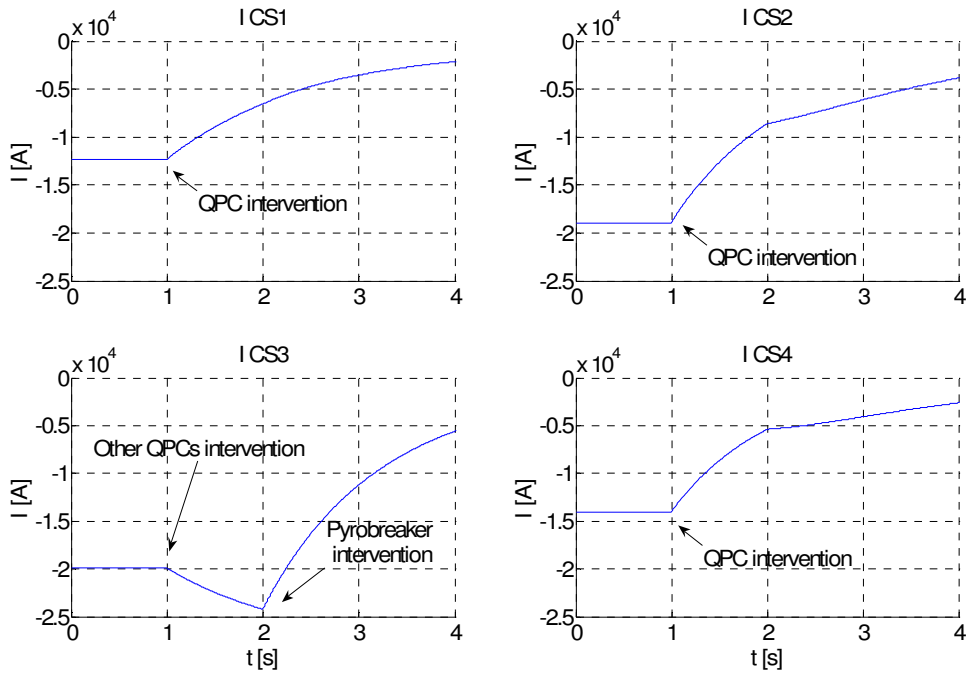

Figure 2.12 - Overcurrent in CS3 coil in case of QPC dc circuit breaker failure

number of possible initial coil current values. It results that the maximum current in case of pyrobreaker operation could exceed the coil rated value. The worst case is showed in Figure 2.12; it refers to the dc circuit breaker failure in the QPC of coil CS3 that leads to a maximum negative current of more than 24 kA before the pyrobreaker intervention. This too large current value could be decreased by reducing the time delay between QPC expected intervention and pyrobreaker activation. For example if this time is halved from 1 s to 0.5 s, the maximum current in coil CS2 would be limited to -22.5 kA.

5 Discussion of results

The studies of the plasma disruption and its effects on the coil overcurrents are quite complex and a large variety of phenomena has been taken into account. The analyses performed so far allowed to verify that the over-currents induced in the CS and EF coils are always positive, reach 3 kA (15% of the nominal coil current) and their amplitude does not significantly depend on plasma parameters such as current derivative, initial current distribution and plasma movement. In fact passive elements (stabilizing plates and vacuum vessel) act as flux conservers that, due to their very low time constants, rapidly move to a resistive current distribution. This means that they have a screen effect on external superconducting coils, whose overcurrent in case of plasma disruption depends only negligibly on plasma behaviour, and that the plasma parameter having a real impact on the coil overcurrent is just the initial current value.

The peak current in the coils has been found adding the calculated coil overcurrent values to the initial coil current values. More than 300 sets of initial current in the coils, obtained from a plasma equilibrium scan, have been considered. The results showed that the peak current in the coils always remained within 5% more than the nominal current. It has however to be pointed out that if other snapshots were proposed, with higher initial current in coils such as EF1 and EF2, where the plasma disruption causes higher over-currents, there would be the possibility of largely exceeding the nominal current value of 20 kA. Anyway it is possible to develop a real time application that, taking in consideration the plasma current and the coil current values in any instant, monitors if the device is running in a safe area or if, in case of plasma disruption, dangerous coil overcurrents could occur, therefore taking the opportune provisions.

The analyses of the QPC operation showed that the intervention of a single QPC can cause too high overcurrents, but this problem can be avoided commanding the QPC all together. On the contrary, in case of failure of the dc circuit breaker of one QPC a significant overcurrent can not be avoided; the worst case is obtained in coil CS3 where the maximum current could reach -24 kA. This value can be limited into an acceptable range by reducing the pyrobreaker activation time from 1 s, as required in the QPC specifications of Table 2.1, to 0.5 s.

It is therefore possible to obtain that the maximum current that poloidal QPCs have to interrupt both in case of plasma disruption and failure of a QPC dc Circuit Breaker is 22.5 kA, and this shall be the reference number for QPC design.

6 Dump resistor value optimization

The poloidal QPC dump resistors have to be designed so as to limit the maximum voltage across the coil under the maximum value of 5 kV and the coil I^2t during a quench event under the maximum tolerable limit of 2 GA^2s. The two requirements have to be suitably balanced, since the maximum I^2t is decreased increasing the resistance value, but this implies an higher voltage across the coil. Due to the mutual coupling between all poloidal coils it is not easy to optimize the QPC resistor value with the certainty that the maximum I^2t and voltage constraints are fulfilled under all possible operating conditions. For this kind of evaluation it is necessary to analyze the behavior of the poloidal circuits taking into account all the mutual coupled elements, and the developed model presented in the previous sections can be easily adapted for this study.

Starting from more than 300 sets of possible coil current initial values already used for the plasma disruption simulation, the poloidal QPC intervention has been simulated taking into account the 1s maximum time delay between the QPC intervention request and the actual intervention. A safe range of poloidal dump resistance values, from 0.25 Ω to 0.15 Ω, have been identified which allows not to exceed the limits, both in terms of voltage and I^2t.

The assumption of a reduced value for the dump resistors permits to design the QPC circuit breaker for a lower reapplied voltage, thus allowing to use a reduced number of series connected components. This would result in an increase of the QPC simplicity and reliability. For this reason it has been decided to select the value of 0.21 Ω for the poloidal dump resistors. This value is reduced in respect with the nominal value of 0.25 Ω showed in Table 2.1.

The simulation of QPC intervention has been performed using the selected dump resistor value under all conditions, including normal QPC operation and pyrobreaker intervention. In each simulated case, the resulting I^2t in the coils remains well under the maximum limit of $2GA^2s$.

It is therefore possible to obtain an optimized set of poloidal QPC specifications, as shown in Table 2.6.

Table 2.6 – QPC optimized rating

Characteristic	Poloidal QPC
Nominal voltage	4.2 [kV]
Nominal current	20 [kA]
Maximum interruptible current	22.5 [kA]
Maximum delay from command	1 [s]

Attachment 2

EXCERPT FROM CONSORZIO RFX INTERNAL NOTE: RFX_BA_TN_08:

Test on turning-on of paralleled IGCTs with low voltage

1 Introduction

In the framework of the Europe and Japan Broader Approach activities in support to ITER, a new Tokamak experiment, called JT60-SA, will be built at Naka, Japan.

Europe will furnish the power supplies and Consorzio RFX will procure the protection system of superconducting coils named "Quench Protection Circuit" (QPC) which has to rapidly zero the current in the superconducting coils in case of quench. In JT_60SA, the maximum coil current value is 26 kA and the maximum reapplied voltage has to remain below 5 kV.

In fusion experiments, the most common solutions for the Protection Circuits are based on vacuum switch with an external counter-pulse network to blow out the arc formed at the contact opening, but at present there is not the availability of a single switch able to sustain the nominal values of 26 kA current in steady state conditions.

Studies have been recently made to identify the most suitable design solution [1]; an alternative approach based on static devices could be attractive: interruption is arcless, very fast and static circuit breakers are almost maintenance-free. In particular IGCT seems to be the most suitable static device, since it is controllable both at turn-on and turn-off and is rated for the largest value of interruptible current. The drawback of this solution is related to the too high on-state losses which represent the main reason they have not been widely used so far.

The hybrid scheme shown in Figure 1-1 was identified and studied; it is composed of a mechanical By-Pass Switch (BPS) connected in parallel to an IGCT static breaker. In normal conditions current flows through the BPS that has negligible resistance. At the BPS opening an arc is formed across its terminals, whose voltage drives current commutation into the static breaker, which then can open without the risk of re-strike when the current commutation is over and the BPS is fully open.

This scheme combines the advantages of the mechanical switch and of the semiconductor; moreover, as proved in [1], the semiconductor can be rated just for the current to be interrupted, thus allowing a full exploitation of the Safe Operating Area (SOA) capability of the large area devices.

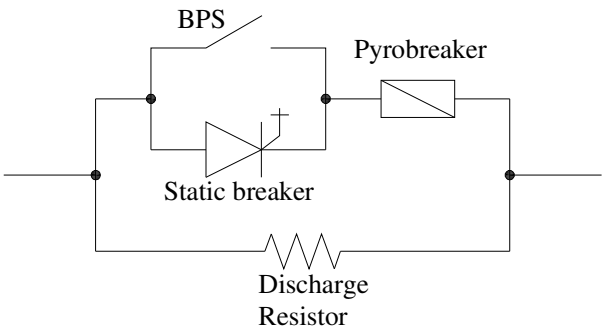

Figure 1-1: QPC hybrid scheme

2 Turning on of paralleled IGCTs

One of the main issues of this hybrid design is related to the static dc circuit breaker turn-on. In fact, due to the high value of the nominal current, it is necessary to foresee the use of paralleled IGCTs. IGCTs require a minimum applied voltage to assure a safe turning-on. If paralleled IGCTs are commanded to turn on, there is the possibility that the first turning-on IGCT imposes its voltage drop, a value generally very small, to all other paralleled IGCTs with the possibility of compromising their safe turning-on. At present time IGCT's manufacturer gives no information about the minimum voltage to be applied to allow a safe turning-on and current sharing of paralleled IGCTs with an high current value.

To deal with this issue, it was devised that a suitable snubber circuit can represents an help for the turning-on of paralleled IGCTs.

In particular the scheme presented in Figure 2-1 includes a diode that has the primary scope of blocking the reverse voltage. When the snubber capacitors are charged and the IGCTs are commanded to turn-on, that diode permits also to avoid that all paralleled capacitors are discharged by the first turning-on IGCT, compromising the turning-on of other IGCTs. This snubber circuit permits to make independent the paralleled IGCTs, whose safe turning-on depends only on the applied voltage.

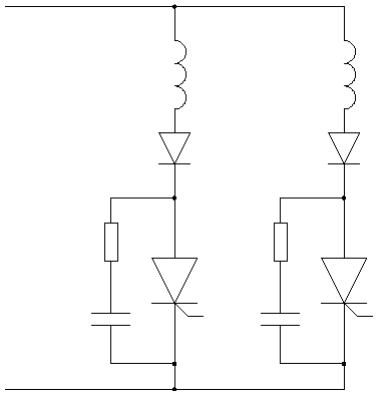

Figure 2-1: Snubber circuit that helps the safe turning-on of paralleled IGCTs

Since the assurance of safe turn-on and current sharing of paralleled IGCTs is a critical aspect in the design of the hybrid circuit breaker, some tests have been performed in order to verify which is the minimum voltage value that assures a simultaneous turning-on of paralleled IGCTs, without the risk that only one has to carry the total current, and the effectiveness of the snubber circuit in maintaining the voltage applied to the IGCTs till their turning-on.

3 Circuit scheme and operation

In order to test and study the turning-on process of paralleled IGCTs with low applied voltage, the circuit represented in the simplified scheme of Figure 3-1 has been implemented.

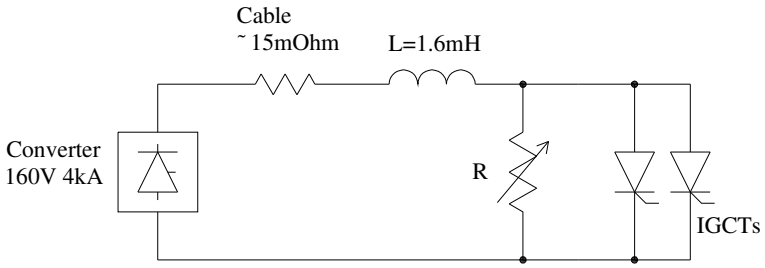

Figure 3-1: Simplified scheme of test circuit

Converter

The converter can operate at full power (I_{max} = 4 kA, V_{max} = 160 V) for a time period of 0.5 s, so the test duration has not to exceed this length of time. The converter maximum current

value guarantees the IGCTs safety because they are rated for a maximum controllable turn-off current I_{TGQM} = 4 kA.

IGCTs

Two paralleled IGCTs (5SHY 35L4512) [1] are used for the tests. They are included in the module that is used at RFX as a spare for the toroidal circuit.

The resistor R

The resistor R connected in parallel to IGCTs is composed of many sectors, each with a resistance value of about 4.5 mΩ.

The sectors were connected in series and in parallel in order to obtain the desired values of current and voltage to study the IGCT turning on and taking in account that the power dissipated has not to lead the resistor temperature over safety values.

The sector section is approximately 75 mm^2 and the length is 400 mm. Considering the specific heat of AISI 316 h_s = 3.08 $J/cm^3°C$, it results that in order not to exceed the over-temperature of 200°C, the current flowing for 1 s has not to exceed 1.8 kA. Considering a maximum current of 4 kA, it is necessary to use at least 3 paralleled sectors. For safety reason blocks of 4 paralleled sectors have been used, connected in series in order to reach the desired resistance value.

Sequence of operation

As indicated in Figure 3-2, with the IGCTs in the status open, the converter is turned on only for the time needed to reach the desired current value. In this period the snubber capacitors paralleled to the IGCTs, are charged to the same voltage of the paralleled resistance R.

At time T1, the converter is turned off and the current keeps flowing through the converter freewheeling diode. After the converter is stopped, the IGCT turning-on is allowed only if the total current value measured at the converter side is smaller than 4 kA. In this way it is not necessary to monitor if the IGCT current exceeds a maximum value, since they are not activated if the current exceeds their maximum controllable turn-off current value, and it is not necessary to foresee the intervention of a protection as a crowbar in case of IGCT overcurrent.

At time T2, the IGCTs are turned on with a voltage applied to them which value can be pre-set by varying the converter current set-point and the resistance R. After the turning-on, part of the current is commutated into the IGCTs branch and then decays to zero with a constant

time varying in dependence of the value of the resistance R and on the on-state IGCT impedances.

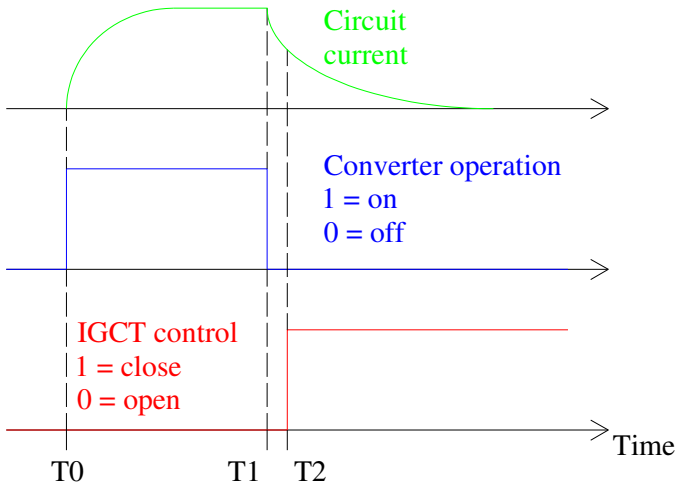

Figure 3-2: Circuit current and control signals

4 Estimation of the IGCT junction temperature during the tests

The estimation of the junction over-temperature can be performed assuming adiabatic condition, because the IGCTs conduct for a time shorter than the heat dissipation constant time even if a very efficient cooling system of the heat sink was assumed. Therefore, the cooling of the heat sink could be useful only to reduce the time between one pulse and the next, but in any case water cooling is not necessary as confirmed by the values of the over-temperature calculated below.

An estimate about the value of I^2t reached by each static component has been worked out: considering as worst case that a single component turns on with an initial current $I_0 = 4$ kA, and assuming the approximate time constant $\tau = 63$ ms for the current decay given by the inductance L and the resistance of the inductance itself and of the cable, the resulting I^2t is $I_0^2 \cdot \tau/2 = 0.51 \cdot 10^6$ A^2s. This value is quite smaller than the limit of $6.1 \cdot 10^6$ A^2s in case of surge indicated in the device data sheet.

An estimate of the temperature reached by the junction during conduction has been worked out using the equivalent electrical model.

Generally [3] the heat conduction processes can be modelled by an equivalent circuit consisting of R/C elements, as illustrated in Figure 4-1, where the heat is equivalent to the current, the thermal resistance and the heat capacity of each layer of the device correspond to

the electrical resistance and capacitance, and the temperature increase of each layer is equivalent to the voltage across the corresponding capacitor.

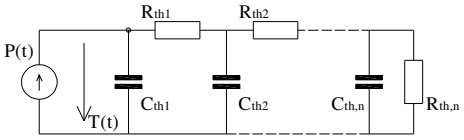

Figure 4-1: Equivalent electrical circuit modelling heat conduction

If the temperature of each internal layer is not of interest and only the junction temperature increase is needed, the simpler equivalent model shown in Figure 4-2 is frequently adopted, where the step response of the thermal impedance can be expressed by the partial fractional representation [*2*]:

$$Z_{th}(t) = \sum_i R_i \left(1 - e^{-t/\tau_i}\right),$$

where R_i and τ_i represent the thermal resistances and the time constants, generally provided on the device data sheet. For the IGCT 5SHY 35L4512 these values for the junction-case (JC) layer are reported in Table 4-1.

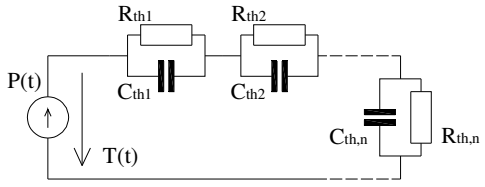

Figure 4-2: Simplified equivalent electrical circuit modelling heat conduction

Table 4-1: Thermal resistances and time constants for IGCT 5SHY 35L4512

Layer	**JC1**	**JC2**	**JC3**	**JC4**
R_i [°C/kW]	5.562	1.527	0.868	0.545
τ_i [s]	0.5119	0.0896	0.0091	0.0024

Assuming for the current generator of Figure 4-2 a waveform with an initial current value of 4 kA which decays with a constant time of 63 ms, the resulting junction temperature variation

is smaller than 11°C, as presented in Figure 4-3, therefore there are no particular over-temperature constraints.

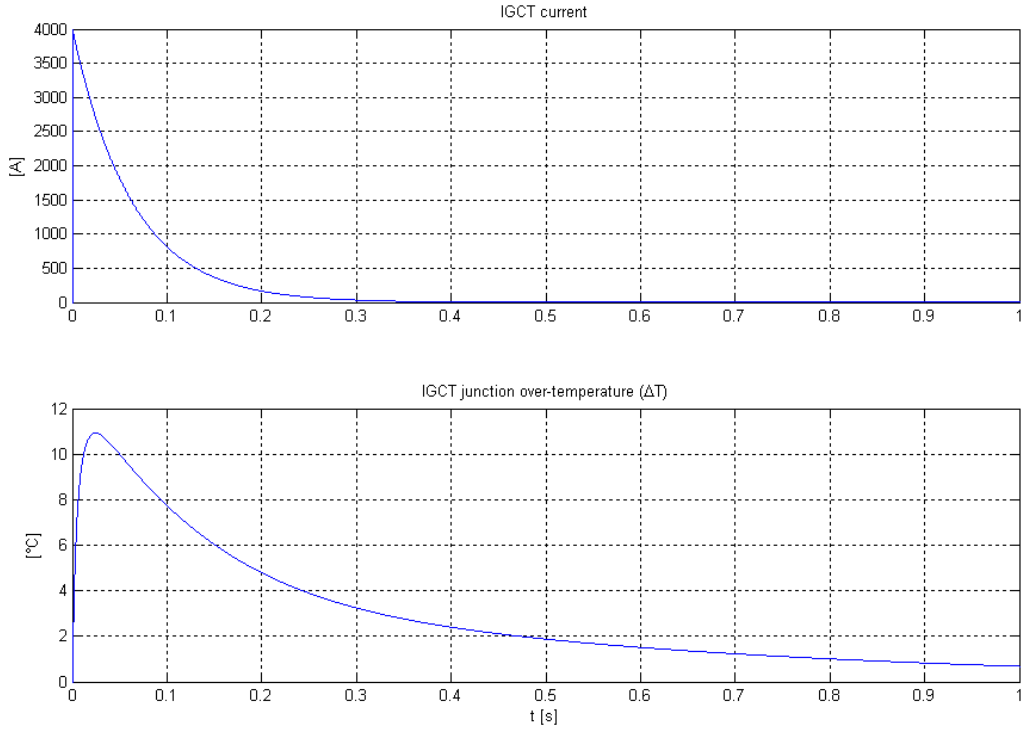

Figure 4-3: ***IGCT Current and Junction temperature variation***

5 Command and control

The turning on command for IGCTs is given by a micro-controller operating according to the following sequence: when the converter is turned on by means of a manual start, a timer is started and after a settable delay time the converter is stopped. After that, the micro-controller checks if the total current is smaller than 4 kA and, if this condition is verified, the turning on commands for the selected IGCTs are generated. The IGCTs are kept in the on state for a settable time.

The scheme on the left of Figure 5-1 represents a sketch of the control signal flow, while the scheme on the right illustrates the working sequence of the micro controller program.

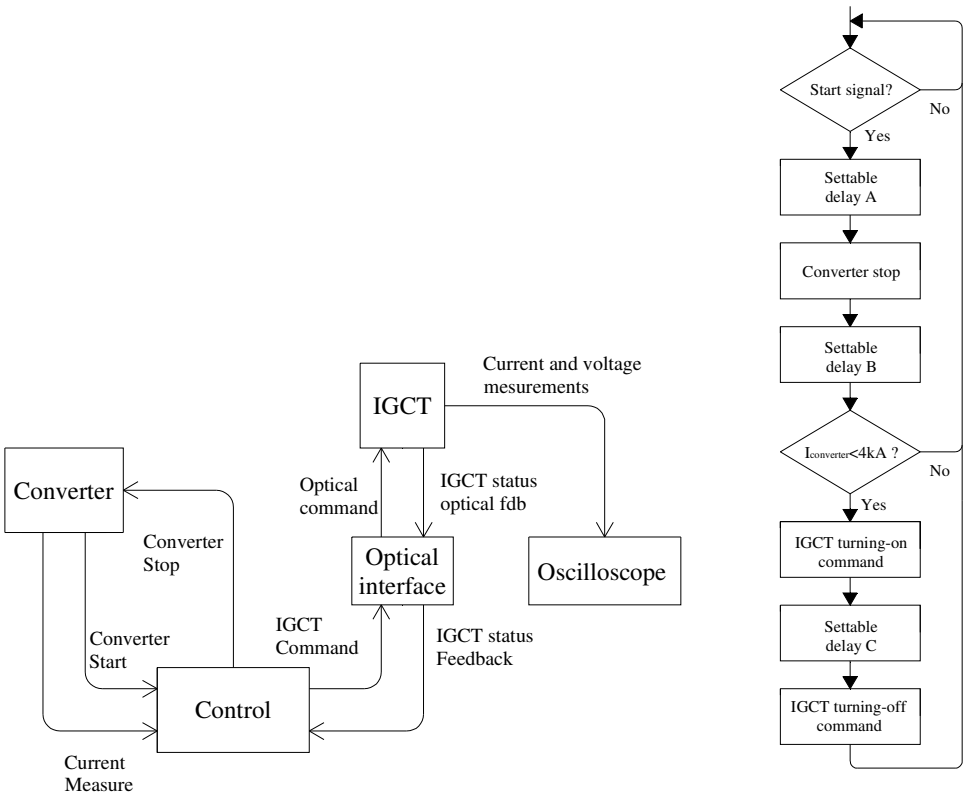

Figure 5-1: Signals connection scheme and Micro-controller program sequence

6 Test results

More than one hundred pulses have been performed, setting different values of converter current and using various resistance values for the paralleled resistor, in order to explore the IGCT turning-on performance with different combinations of initial current and voltage values, and to find a minimum voltage value that permits to turn on the paralleled IGCTs without problems.

The complete list of the tests performed is reported in Table 6-1, where also the details about the current reached at the time of turning on, the maximum current in the IGCTs, the IGCT voltage at the time of turning-on and the IGCT status are reported.

The IGCTs current and voltage waveforms in the different pulses are very similar, an example is reported in Figure 6-1 and in Figure 6-2. In the last, the zoomed IGCT voltages during turning-on are shown; the turning-on of the two paralleled IGCTs can be considered simultaneous, since the jitter between them is not appreciable with the oscilloscope resolution of 100 ns highlighted in the figure with the dots.

The turn-on voltage and the maximum current of the IGCTs in the pulses performed are also summarized in the plot diagram of Figure 6-3.

Discussion of the results

A good turn-on of both the IGCTs was always observed with applied voltages higher than 1.5V, as summarized in Table 6-1.

In all cases the two paralleled IGCTs have proved a contemporaneous turning-on, like that shown in Figure 6-2. Moreover the current unbalance between the two paralleled IGCTs never exceeds 10% of the current value.

The last two groups of pulses are repeated, in order to evaluate the turn-on repeatability. They proved the reliability of the turning-on of paralleled IGCTs in two operating conditions.

It was not possible to perform tests with higher values of the initial current and similar voltage applied, because this condition requires to reduce the resistance R up to values so lower than the IGCTs on-state resistance that the percentage of the current commutated to the IGCTs becomes quite low. In any case, the significance of the tests is not reduced, because if a reliable turn-on is demonstrated in a current range from few amperes to about five hundred amperes, it is quite admissible to extend the results to higher initial IGCT current values and same voltages applied.

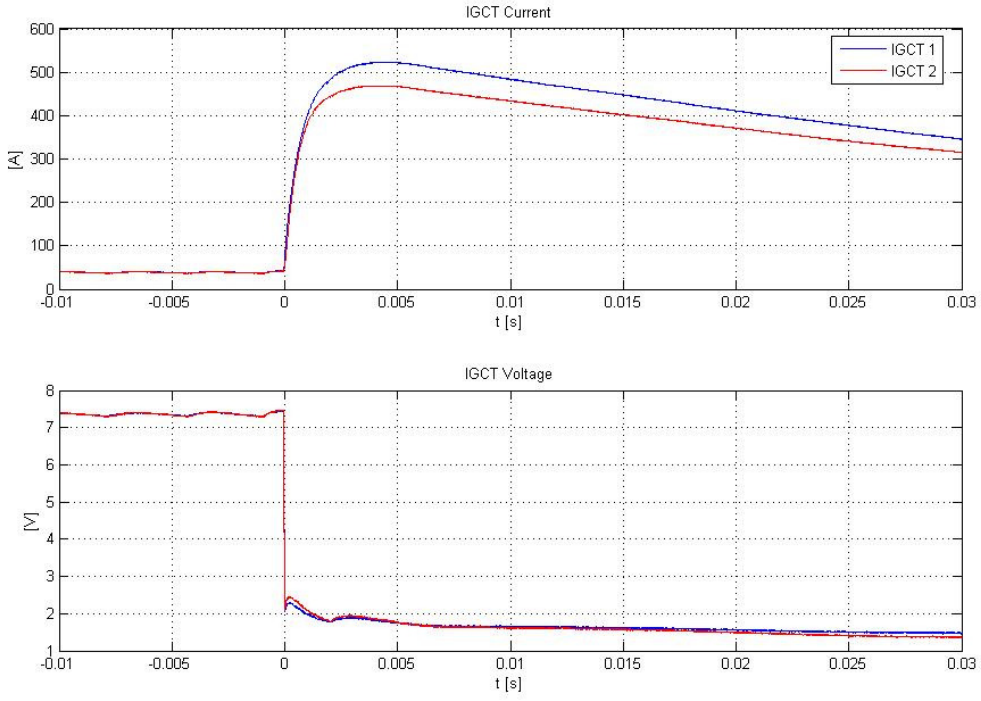

Figure 6-1: IGCT voltage and current typical waveforms

Table 6-1: List of test pulses

Pulse		Converter	IGCT	Maximum current	IGCT Status
Date	Number	Current [A]	Voltage [V]	in IGCTs [A]	
06/09/2007	1	340			Not connected
	2	360			Not connected
	3	350	25	100	Turned on
	4	350	25	100	Turned on
	5	350	25	100	Turned on
	6	340	26,6	200	Turned on
07/09/2007	1	383	26,6	200	Turned on
	2				Measure problem
	3	340	25	200	Turned on
	4	340	26	200	Turned on
10/09/2007	1	360	25	150	Turned on
	2	740	50	330	Turned on
	3	700	49	300	Turned on
	4	340	25	140	Turned on
	5	416	10,5	140	Turned on
	6	436	10,6	150	Turned on
	7	724	19,5	290	Turned on
	8	800	20	305	Turned on
	9	800	7,4	215	Turned on
	10	800	7,2	208	Turned on
	11	456	4	91	Turned on
	12	450	4	91	Turned on
	14	Measure problem	2,6	41	Turned on
	15	316	2,7	50	Turned on
11/09/2007	1	832	3,6	133	Turned on
	2	832	3,5	133	Turned on
	3	650	2,6	87,5	Turned on
	4	650	2,6	83	Turned on
	5	450	1,9	35	Turned on

	6	450	1,9	35	Turned on
	7	450	1,9	33	Turned on
	8	450	1,9	37	Turned on
	9	450	1,9	33	Turned on
	10	?	1,4?	-	(*)Turn on problem
	11	330	1,4	12	Turned on
	12	330	1,4	12	Turned on
	13	?	1,4?	-	(*)Turn on problem
	14	880	2	83	Turned on
	15	1500	3,6	177	Turned on
	16	1550	3,7	197	Turned on
	17	1216	3,1	137	Turned on
	18	866	2	50	Turned on
	19	633	1,5	20	Turned on
	20	600	1,5	20	Turned on
	21	616	1,5	18	Turned on
	22	600	1,5	20	Turned on
	23	500	1,3	9	Turned on
	24	550	1,3	8	Turned on
	25	500	1,3	9	Turned on
	26	550	1,3	8	Turned on
	27	480	1,1	4	Turned on
	28	?	1,1		(*)Turn on problem
17/09/2007	1	?	2,1	55	Turned on
	2	900	2,2	58	Turned on
	3	1400	3,7	193	Turned on
	4	1630	4,3	230	Turned on
	5	2030	4,6	325	Turned on
	6	2030	4,6	330	Turned on
	7	2400	6,6	400	Turned on
	8	2500	6,8	450	Turned on
19/09/2007	1 - 30	2000	5	300	Turned on
	31 - 42	2800	7,2	450	Turned on

(*) Since the oscilloscope was triggered on the IGCT current signal, the available record in those cases is not related to the time period of the turn on command but to a following time period when the total current is already zero. That is the reason why the converter current and

the IGCT voltage of those cases are reported with a question mark: these values, in fact, are not obtained from direct measurements, but are the values obtained in pulses with similar pre-settings.

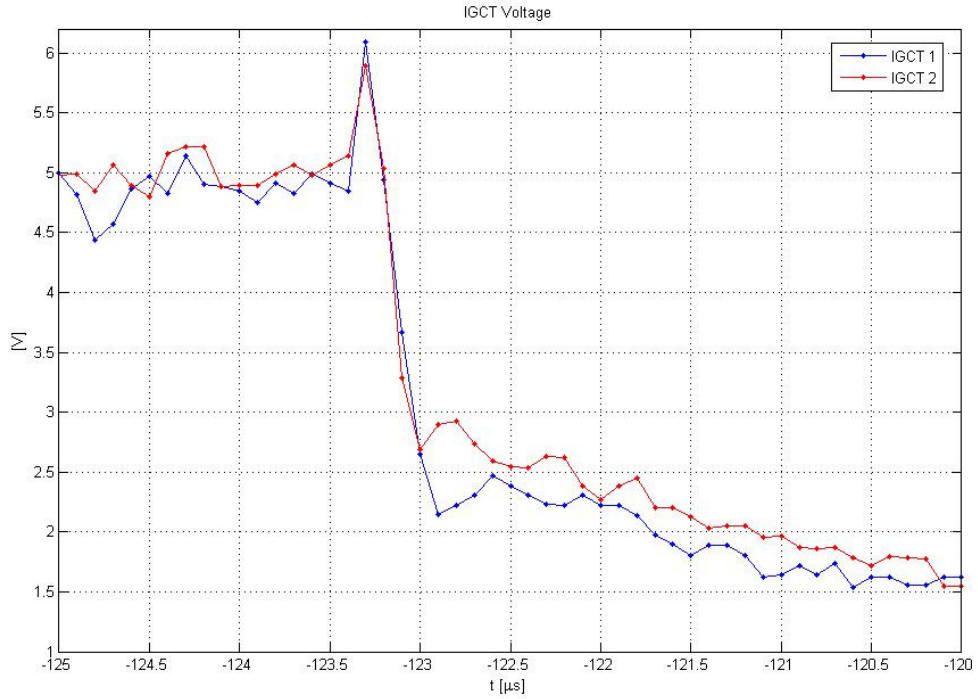

Figure 6-2: IGCT voltage during turning-on

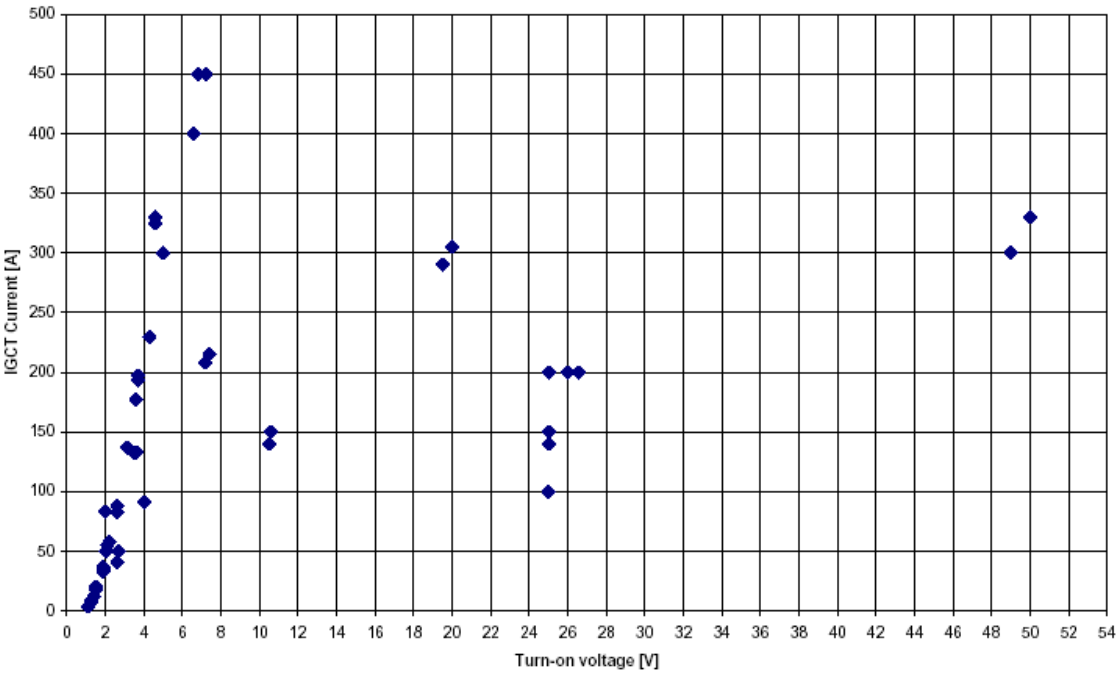

Figure 6-3: Turn-on voltage and maximum current of IGCTs on performed pulses

7 Conclusions

The results of the tests performed showed that the two paralleled IGCTs have always turned-on contemporaneously with an applied voltage across them of at least 1.5 V. The current unbalance between the two paralleled IGCT has never exceeded 10% of the current value.

The reliability of the simultaneous turning-on of paralleled IGCTs has been demonstrated in repetitive pulses with applied voltages of 5 and 7.2 V and initial current values in the IGCTs of 300 and 450 A respectively.

These voltage values are certainly lower than the arc voltage of the bypass switch which is applied to the IGCTs in the hybrid circuit breaker proposed for the JT60SA Quench Protection System, therefore these tests prove the feasibility of this design solution as far as the issue related to the safe turn-on of the IGCTs in parallel is concerned.

8 References

[1] R. Piovan, E. Gaio, L.Novello: “Performance analysis of a hybrid IGCTS- mechanical dc circuit breaker for SC magnet quench protection”, 22nd SOFE Albuquerque - New Mexico (USA) – 17 - 22 June 2007,

[2] Datasheet ABB IGCT 5SHY-35L4512.

[3] N. Mohan, T.M. Undeland, and W.P. Robbins, Power Electronics, 2nd ed., John Wiley & Sons Inc, USA, 1989, pp. 730-743

Attachment 3

EXCERPT FROM CONSORZIO RFX INTERNAL NOTE RFX_BA_TN_18:

Development of a 10 kA prototype of Hybrid Mechanical-Static Circuit Breaker

1 Reasons for developing a prototype

The most innovative part of the QPC is represented by the Hybrid Mechanical-Static Circuit Breaker. In fact the combination of a mechanical By-Pass Switch (BPS) with a IGCT static Circuit Breaker (CB) has never been used for conducting and interrupting high current values up to the values needed for the QPC of JT-60SA.

An open issue resulting from the integration of the mechanical BPS and the static CB technologies refers to the reliability of current commutation between the two elements.

The correct operation of the Hybrid CB requires that the voltage of the arc current appearing at the BPS terminals when it starts opening is able not only to turn-on the IGCTs connected in parallel, but also to drive the complete current commutation from the BPS to the static devices. In fact, as the current is increasing in the Static CB, also the voltage drop across it will increase and there is not enough confidence that the arc voltage is sufficient to complete the current commutation process.

No experience is available on this field: as presented in Chapter 3, some experimental tests have been successfully performed using two IGCTs connected in parallel to a resistor, but they were mainly aimed at evaluating the possibility of having a safe turn-on of more paralleled IGCTs with low voltage applied, so as to assess the feasibility of the hybrid CB concept based on IGCT technology.

Therefore, the study of the behaviour of the arc voltage and of the current commutation represents a key point for the assessment of the reliability of the hybrid CB operation, that can be suitably investigated only by means of experimental tests.

For these reasons it has been decided to develop a prototype of the QPC Hybrid CB, whose operation will permit to gain experience on the current commutation from the mechanical BPS to the Static CB and to test the reliability of such technical solution, possibly learning how to improve it.

2 The Prototype

A prototype of the QPC Hybrid CB has been set up at Consorzio RFX connecting in parallel a mechanical BPS and a static CB based on IGCT technology.

2.1 The Mechanical BPS

The Mechanical BPS used for the prototype is shown in **Error! Reference source not found.**. This is the mechanical BPS used for ITER tests [20]. It is rated for a nominal current of 60 kA dc continuous and a nominal voltage of 17.5 kV. It is provided with 12 contacts, 6 of them located in the upper part and the remaining 6 in the lower part. Each contact consists in a main contact in parallel to a sacrificial contact. The main contacts have a lower contact impedance, therefore when the BPS is closed the majority of the current passes through them. When the BPS is commanded to open, the opening of sacrificial contacts requires a time longer than the opening of the main contacts. This means that when the BPS is opening the current commutates from the main contacts to the sacrificial

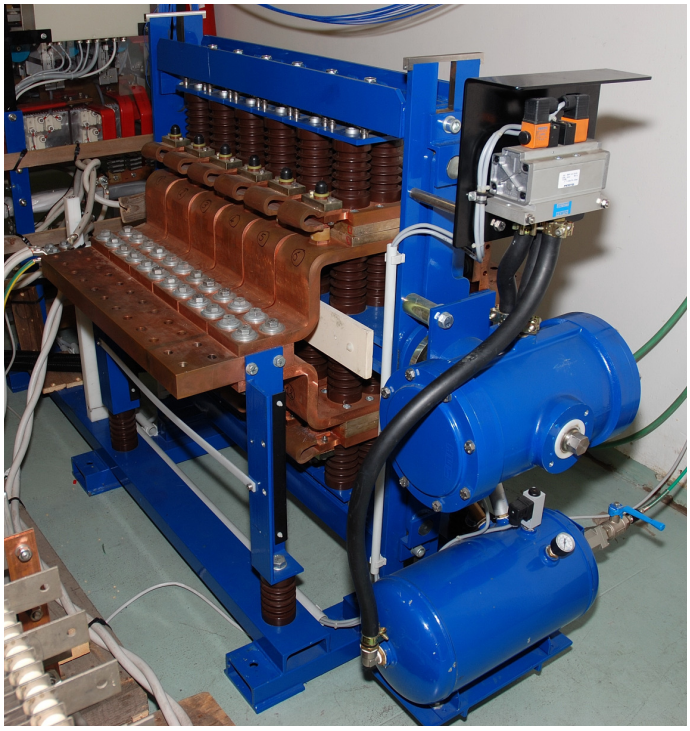

Figure 4.1 – Picture of the BPS used for the Hybrid CB prototype

contacts and the arc is formed across the latter ones. This permits to operate the BPS preserving the main contacts and the routine maintenance can be performed only on the sacrificial contacts, with a save of money and time.

The whole resistance of BPS in closed status is less than 1 μΩ.

The BPS is opened by a pneumatic actuator, operating at a pressure of 6 bar. The delay between the opening command and the beginning of the opening is about 230 ms. This delay is due to the pneumatic actuator and to the mechanical inertia of the BPS (the total weigth of the BPS is about 2000 kg). When the distance between contacts is about 20 mm a micro-switch commutates its position, signaling the BPS open status. This happens about 350 ms after the opening command. Finally, about 450 ms after the opening command, the BPS is completely opened with a contact distance of about 50 mm.

2.2 The Static CB

The Static CB used for the prototype, is a static current interruption module supplied by Ansaldo for the toroidal circuit of RFX [29].

It is composed of 3 paralleled IGCT 5SHY32L4512, provided with snubbers for current derivative limitation during turn-on and voltage clamp during turn-off. A diode for blocking inverse voltage is connected in series to each IGCT.

The Static CB is able to interrupt unidirectional dc current up to 10kA, with a maximum voltage of 4 kV (maximum no load voltage without commutation). It is designed for a duty cycle of 0.5 s every 10 minutes.

The current in each IGCT can be measured by means of shunt resistors that have also the aim of assuring a good current sharing between the three devices.

3 The Test Circuit

A test circuit for operating the Hybrid CB prototype has been set up at the Consorzio RFX laboratory. A simplified scheme is shown in Figure 4.2, a picture of the test circuit is shown in.

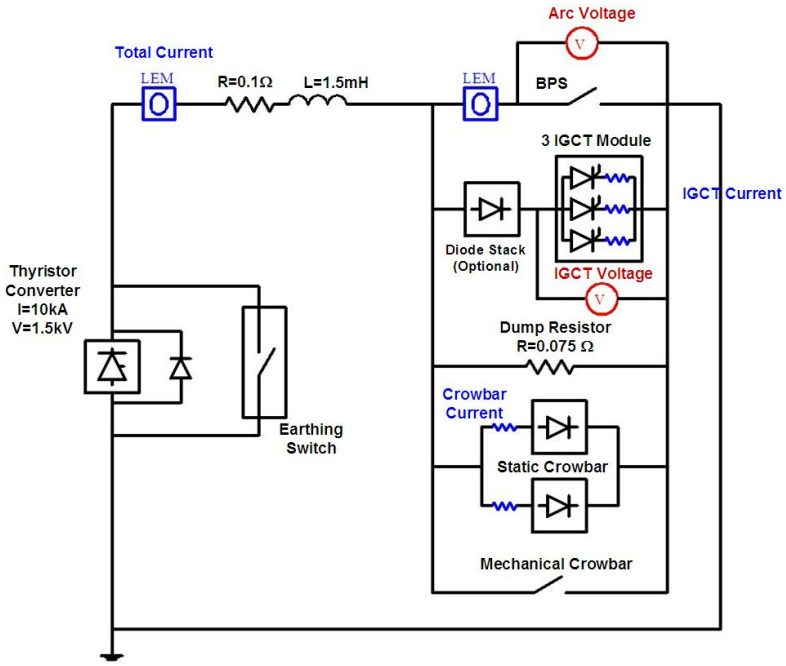

Figure 4.2 – Electrical scheme of the test circuit set up at Consorzio RFX

A current up to 10 kA is supplied by a thyristor converter rated for 16 kA and 1.5 kV, normally used for supplying the toroidal circuit of RFX, into the series connection of a resistor (R = 0.1 Ω), an inductance (L = 1.5 mH) and the Hybrid CB prototype. A discharge resistor of 75 mΩ, simulating the QPC dump resistor, provides the commutation path for the current after the Hybrid CB opening.

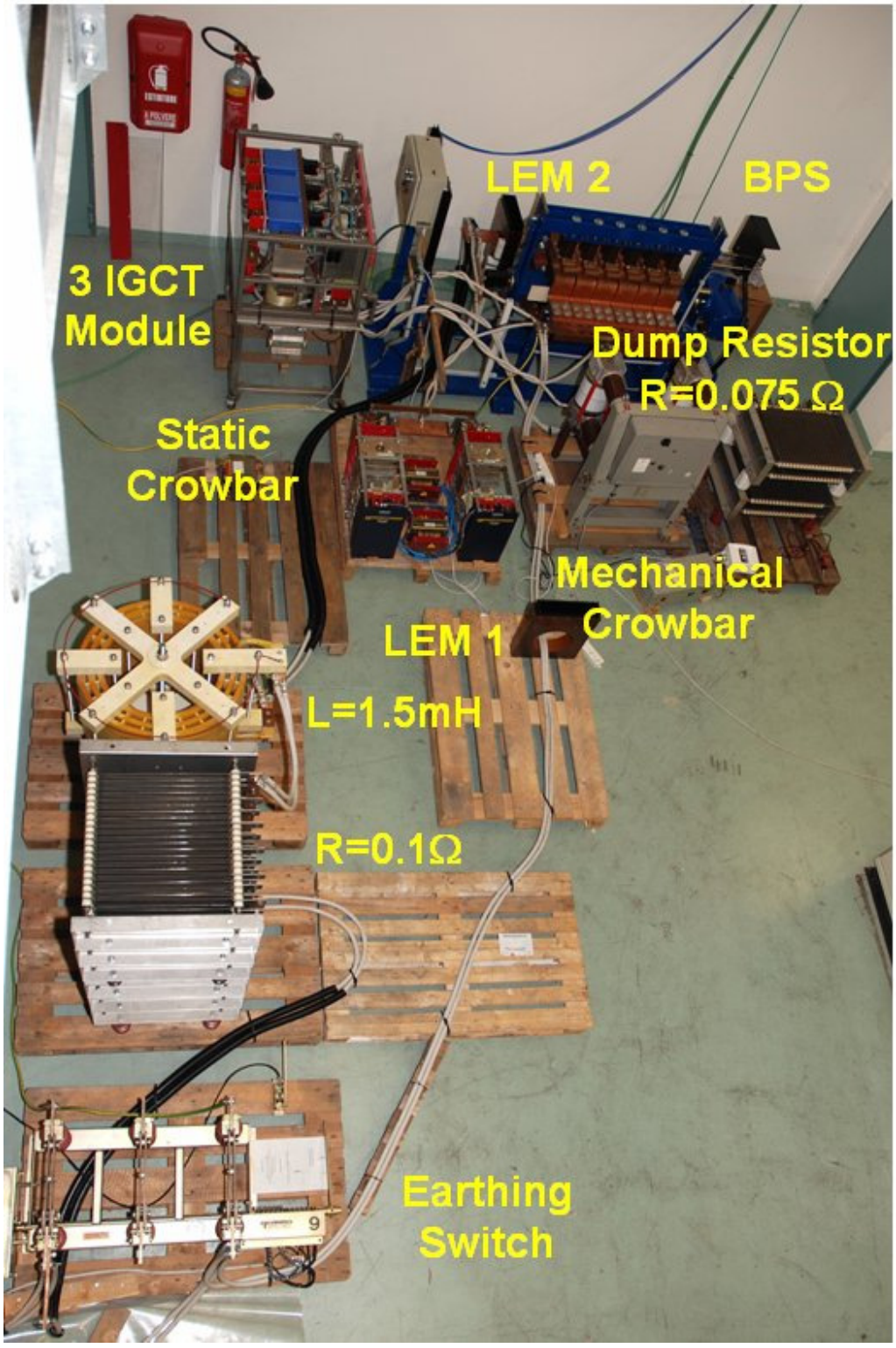

Figure 4.3 – Picture of the test circuit set up at Consorzio RFX

A making switch is connected in parallel to the Hybrid CB, in order to provide a low impedance path for the current in case of mis-operation of the Hybrid CB. This making switch is composed of a static crowbar connected in parallel to a mechanical switch. The static crowbar, consisting in two paralleled Gate Turn Off Thyristors (GTO) 211QS26923B, allows for a very rapid intervention of the

making switch (in the order of micro seconds) but with limited I^2t capacity, while the mechanical switch has slow intervention time (in the order of 30 ms) but higher I^2t capacity.

4 The Control

The operation of all the test circuit devices is coordinated by a very fast control system that performs also fault detection and protection intervention.

This system has been implemented using a Field Programmable Gate Array (FPGA) control board that has been programmed so that it receives as inputs the status of the circuit power components and the current and voltage measurements acquired from the field and it generates in real-time the commands for performing the desired operation sequence.

The current and voltage measurements shown in **Error! Reference source not found.** and listed in Table 4.1 are at first normalized into 0-10 V signals, then converted in optical signals by means of opto-electronic interfaces that permit to insulate the control from the power part and finally sent to the control system where they are re-converted into 0-10 V signals that are monitored in real time during the pulse by the control system.

Table 4.1 – Acquired Measurements

Measure	Name	Range	Transducer
Total current	I TOT	0 - 10 kA	LEM
BPS current	I BPS	0 - 10 kA	LEM
IGCT current	I IGCT 1,2,3	0 - 4 kA	Resistive shunts
GTO current	I GTO 1,2	0 – 8 kA	Resistive shunts
Total Voltage	V TOT	0 – 1 kV	Voltage divider
BPS arc voltage	V BPS	0 – 50 V	Voltage divider with clamp
IGCT voltage	V IGCT 1,2,3	0 – 1 kV	Voltage divider
Converter current	I CONV	0 – 16 kA	Resistive shunt
Converter	V CON	0 – 1.5 kV	Voltage divider

Voltage

In order to guarantee the safe operation of the test circuit it is necessary to monitor in real time that all the safety limits in terms of current, voltage and I^2t are not exceeded and that the status of the components is correct according to the operation sequence. Since the FPGA system used for performing control is very fast (the time cycle is less than 20 ns) and it permits to monitor in real-time the components' status and the current and voltage measurements, it has used also for performing fault detection and protection intervention.

The list of the main detected faults is shown in Table 4.2. In case of fault the control system automatically performs a protective sequence consisting in turning-off the thyristor converter and closing the crowbar. This permits to by-pass the hybrid CB prototype so as to create a low impedance path for the current that avoid the onset of dangerous situations for the mechanical switch and the static module. Moreover the turn-off of the converter assures that the current flowing in the test circuit rapidly decreases to zero with the time constant of 15ms imposed by the series connected resistor and inductance.

Table 4.2 – Main Alarms

Alarm	**Description**
BPS status not ok	The BPS remains closed after opening command
IGCT status not ok	The IGCT status does not match the IGCT turn-on and turn-off commands
BPS current restrike	Some time after BPS opening command the current in BPS is not zero
Current commutation failure	Some time after IGCT turn-on the current is not completely commutated in IGCTs
Current for too long time in IGCTs	Some time after IGCT turn-off the current in IGCT is not zero
Max I^2t in IGCT	The I^2t in one IGCT is exceeding a set limit
Maximum current in IGCT	Current in one IGCT is exceeding a set limit
Maximum current	Total current is exceeding a set limit

Maximum voltage	Total voltage is exceeding a set limit

5 Operation sequence

Before the starting of the pulse sequence, the converter is off, the BPS is closed, the IGCTs are turned-off and the crowbar is open.

At the beginning the converter is turned-on and it starts to supply the predefined current. When the current reaches the desired value the BPS opening command and the IGCT turn-on command are generated. When the BPS is completely open and the current is transferred into the IGCTs the converter is turned off, the IGCT are turned off and the current starts to commutate in the paralleled resistor.

A simplified scheme of the operation sequence is shown in Figure 4.4. The sequence is managed on the basis of pre-settable times, so that it is possible to change the operation sequence before performing the pulse.

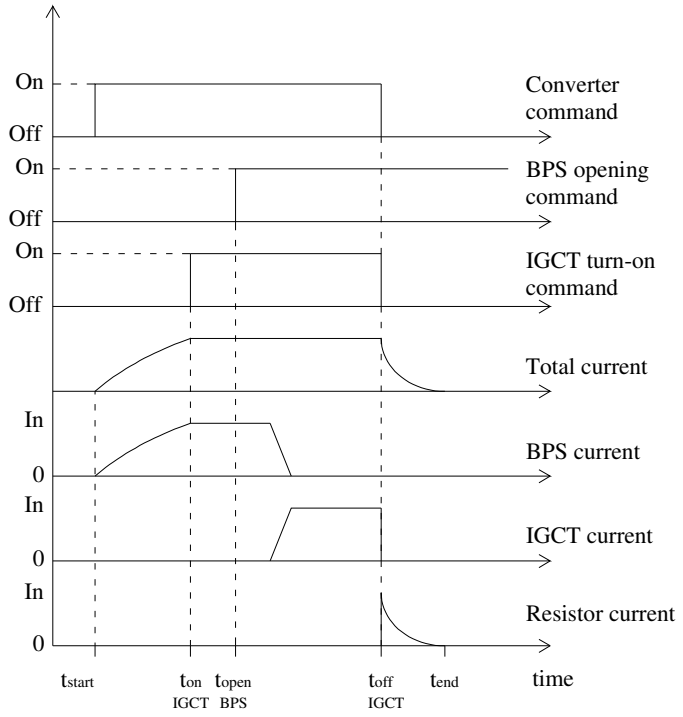

Times

t_{start}: Converter turn-on;

$t_{on\ IGCT}$: IGCT turn-on;

$t_{open\ BPS}$: BPS opening command;

$t_{off\ IGCT}$: IGCT turn-off and converter turn-off;

t_{end}: end of pulse

Figure 4.4 – Normal operation sequence

6 High current interruption tests

The prototype was used with a maximum current of 7 kA. The results obtained in case of commutation and interruption of a current of 7 kA are shown in Figure 4.5 and Figure 4.6.

The BPS and the IGCTs are commanded to open and to turn-on, respectively, at the same time t=50 ms. The contacts of BPS start to separate at t=280 ms and an arc is formed, whose voltage drives the current commutation from the BPS to the IGCTs.

The current commutation has a duration of 4 ms, a time that permits the arc voltage to reach the maximum value of 24 V. At time t=284 ms all the current is commutated into the IGCTs and the arc is extinguished: the voltage at the BPS terminals is the voltage drop across the IGCT module that is about 20 V. The IGCTs turn-on simultaneously without problems and the current sharing between them is very good, with a current unbalance lower than 3% of the total current. There is a difference of about 250 A between the IGCT current and the total current. This difference is the current flowing in the 75 mΩ resistor connected in parallel to the IGCTs, due to the IGCT module voltage drop.

When the BPS is completely open at t=400 ms the IGCTs are commanded to turn-off and the current is commutated into the discharge resistor with a reapplied voltage of 500 V. The dielectric insulation of the BPS contacts is guaranteed by the sufficient distance of 50 mm and no current re-strike appears across them.

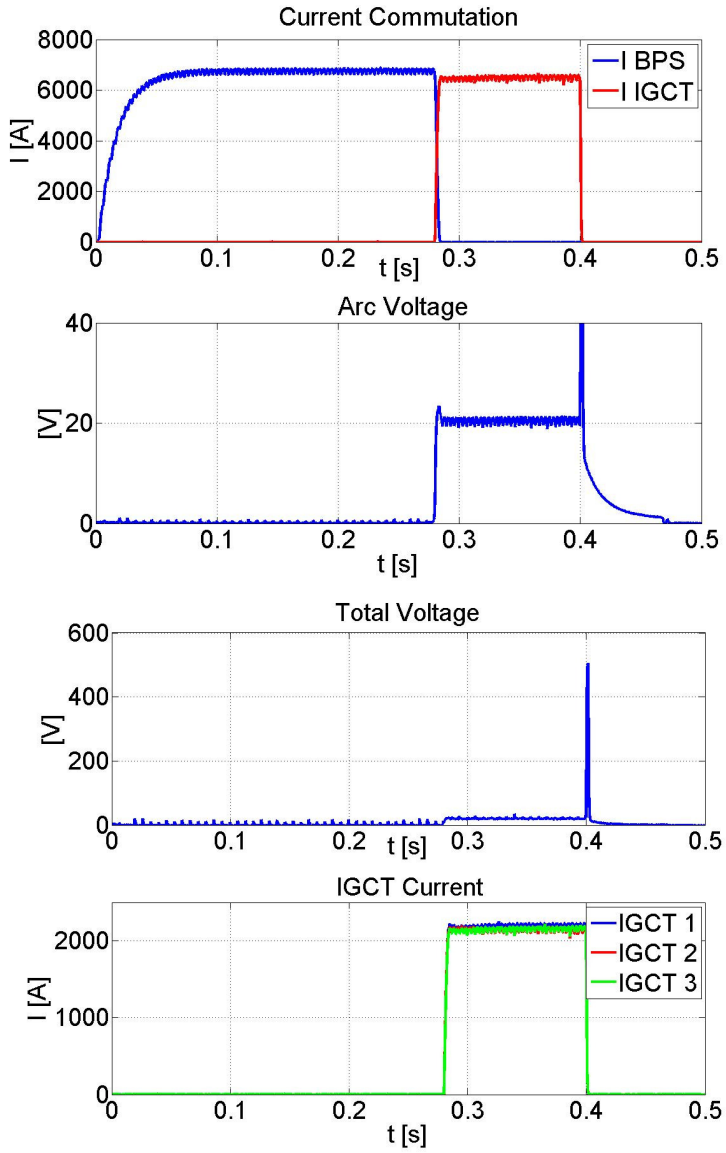

Figure 4.5 – Results of commutation and interruption of 7 kA current

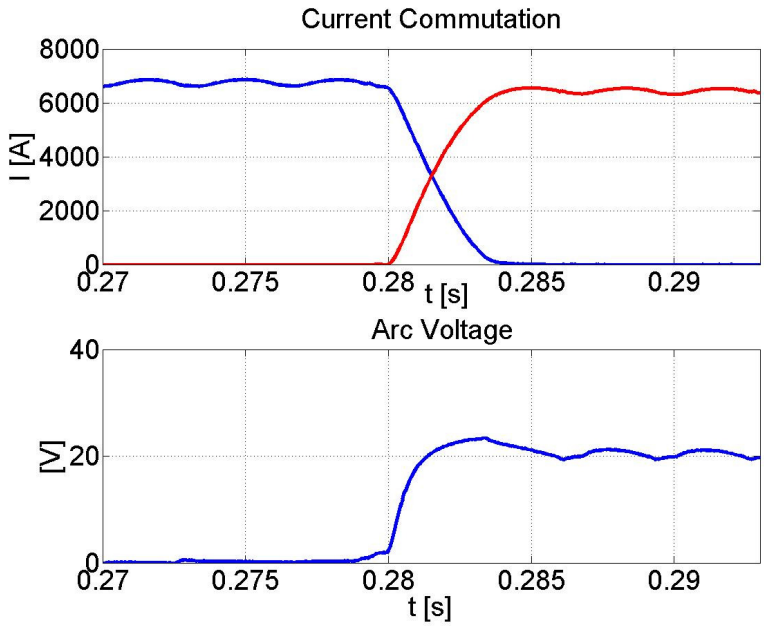

Figure 4.6 – Zoom of 7 kA current commutation

7 Arc voltage test

The voltage drop across the IGCT module is due to the IGCT impedance, the blocking diode impedance and the shunt resistor for current measurement. With a current in each branch of 2.3 kA the resulting voltage drop is about 20 V. With a higher current the voltage drop across each branch of the static module would be higher and there is the possibility that the arc voltage is not sufficient to completely commutate the current from the BPS to the IGCTs, causing a persistence of the arc. In this case it is not possible to interrupt the current, in fact when the IGCTs are turned off the current would be re-commutated in the BPS, preventing the current interruption. In order to investigate the arc voltage behavior during BPS opening without current commutation some pulses have been performed introducing an intentional delay in the IGCT turn-on command. In the pulse whose waveforms are shown in Figure 4.7, the BPS is commanded to open at t=50 ms, its contacts start moving at t=279 ms but the IGCTs are commanded to turn on only 16 ms after arc current creation at the BPS terminals, at t=295 ms.

During the first milliseconds, the arc voltage appearing when the BPS contacts start separating has the same waveform observed in the pulses where the IGCT are already turned-on at BPS opening and the current commutation is occurring, but in this case the current commutation is not possible and the arc voltage keeps on increasing since the distance between BPS terminals is increasing. When the IGCT are finally turned on, the arc voltage has reached a value of about 35 V.

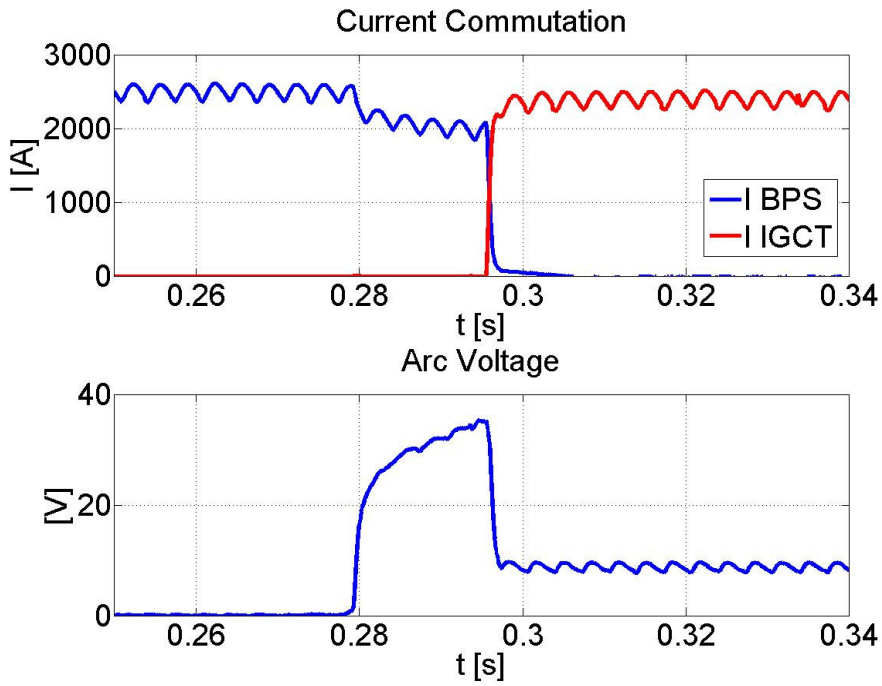

Figure 4.7 – Results of current commutation with a 16 ms delayed IGCT turn-on

The observed increase of arc voltage permits to assess the reliability of current commutation from the mechanical BPS to the static CB, that represented one of the most important aspect to be studied in deep detail.

In fact, as the current in the Static CB is increasing, also the voltage drop across it will increase and it is possible that the initial arc voltage is not sufficient to drive the complete current commutation. Fortunately, as the BPS contacts are separating, also the arc voltage increases, helping the current commutation process.

Of course it is not possible to have too high voltage drop across the static CB, otherwise the current commutation will last a long time, speeding up the BPS contact wearing, with the extreme case of failure of current commutation. For this reason not only the impedance of the Static CB, but also the stray inductances related to the connection with the BPS should be minimized.

8 Discussion of results

More than one hundred pulses have been performed with the Hybrid dc CB prototype, with current values up to 7 kA.

In all performed pulses a rapid and complete current commutation from the BPS to the static CB has been observed, followed by current interruption performed by static CB without BPS arc restrike. This result represents an experimental assessment about the reliability of the Hybrid CB proposed as solution for the CB of JT-60SA QPC.

In both pulses where the IGCT turn-on command was issued before BPS opening and after it, all the three IGCTs start conducting with a good current sharing also in dynamic condition. Therefore, from the point of view of optimizing the IGCT turn-on sequence, it is not possible to identify a preferable solution between issuing the IGCT turn-on command before or after BPS opening time. Conversely, from the point of view of minimizing the arc current duration across the BPS contacts and consequently reducing the contact wearing, it is better to turn-on the IGCTs before the arc formation. Since no current is observed in IGCTs before the effective BPS opening, it is possible to simplify as much as possible the operation sequence, issuing simultaneously the BPS opening command and the IGCT turn-on command.

Attachment 4

EXCERPT FROM CONSORZIO RFX INTERNAL NOTE: RFX_BA_TN_32: Design and set up of the Test Facility to test the ByPass Switch prototype of the JT-60SA Quench Protection Circuits

Introduction

In the framework of the contract for the procurement of the Quench Protection Circuits (QPC) for the JT-60SA satellite Tokamak, awarded to the company Ansaldo Sistemi Industriali by Italian National Research Council, acting through Consorzio RFX, it was agreed to perform part of the type tests on the prototypes of the QPC components at Consorzio RFX.

This document presents the design and set up of the test facility.

1 Aims of the ByPass Switch test facility

The facility set up at Consorzio RFX has the aim to perform the factory type tests on the BPS, as described in the paragraph 5.2.1 of the Technical Specifications **Error! Reference source not found.**.

The tests which was agreed to be performed at Consorzio RFX are:

1. Tests to verify the electro-dynamic resistance of the BPS;
2. Tests to verify the electric wear of the sacrificial contacts of the BPS.

1.1 Test Facility requirements

The tests requirements are:

- DC current up to 51.4kA for at least 100ms;
- DC current up to 25.7kA to be kept constant for the time needed to perform the commutation;
- A suitable control system and data acquisition system;

2 Test Circuit Design

2.1 Test Circuit Elements

The test circuit exploits part of the RFX-mod plant, as described in the following paragraphs.

The electrical scheme is shown in Figure 4:

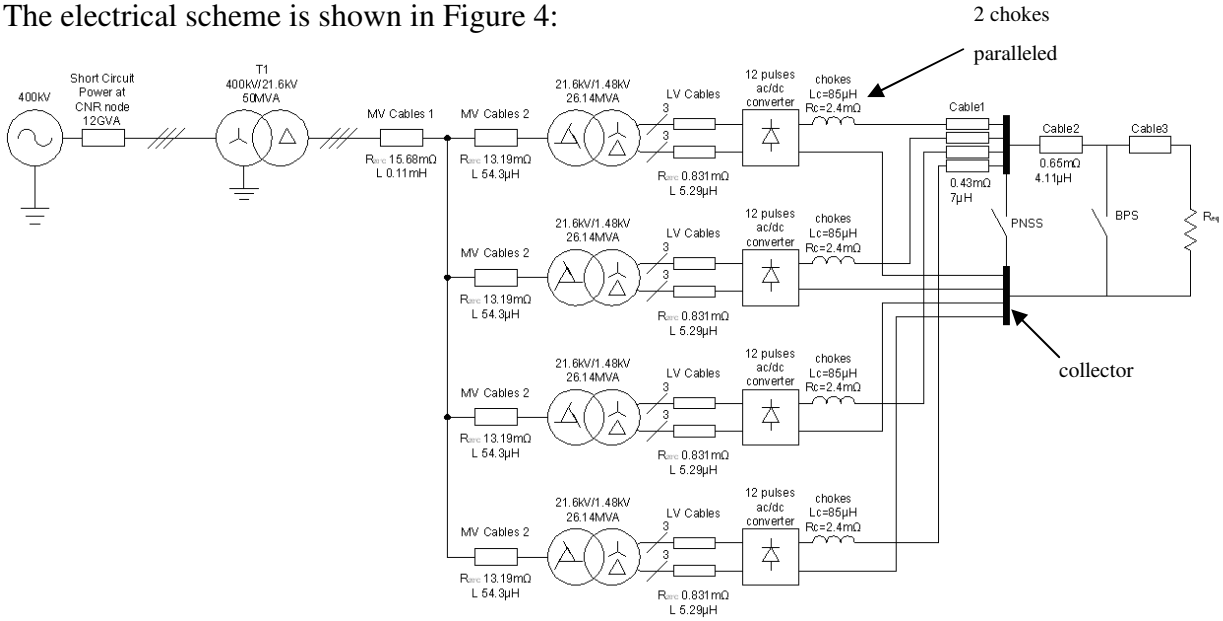

Figure 4 – Electrical scheme

From the left:

- 400kV grid with a shortcircuit power of 12GVA;
- T1 step-down transformer;
- Medium voltage cable from T1 to the medium voltage switchgear;
- Medium voltage cable from the medium voltage switchgear to the transformer of the converters;
- The step-down transformers with the delta extended primary winding;
- The cables from the transformers to the bridges;
- The four 12 pulses bridges;
- The chokes;
- The cables from the chokes to the collector;
- The collector (which can be shortcircuited by the PNSS);
- The cables from the collector to the BPS;

- The BPS;
- The cables from the BPS to the equivalent resistor;
- The equivalent resistor.

2.1.1 ac/dc converters

The ac/dc converters named “A Unit” are composed of two sub-unit with the characteristics listed in Table 2:

Table 2 – Sub-unit characteristics

Sub Unit Ratings		
No load voltage	2000 V	
Load voltage	1350 V	
DC current	6.250 kA	8.124 kA
Duty Cycle	5/600 s	0.5/600 s
Ground insulation	12kV rms	
N. Thyristors	12	
Cooling	Natural air	

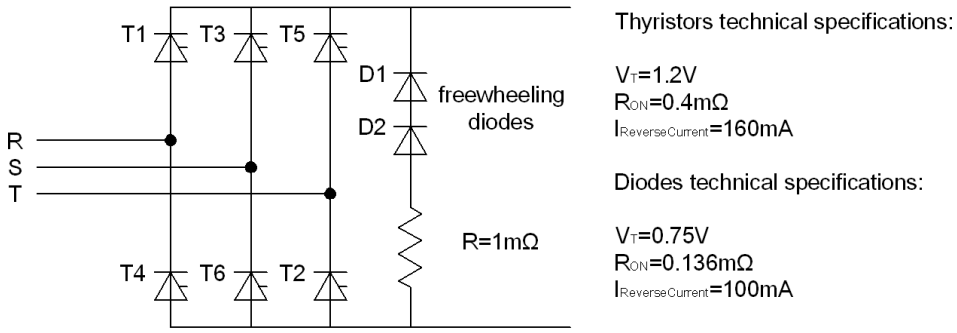

Figure 5 – Subunit electrical scheme

Each sub-unit is composed of a transformer with a delta extended primary winding and a delta or star secondary winding which supplies two paralleled 6 pulses thyristor bridges. The subunits can be used independently or in series or in parallel.

The simplified electrical scheme of an “A unit” is presented in Figure 6:

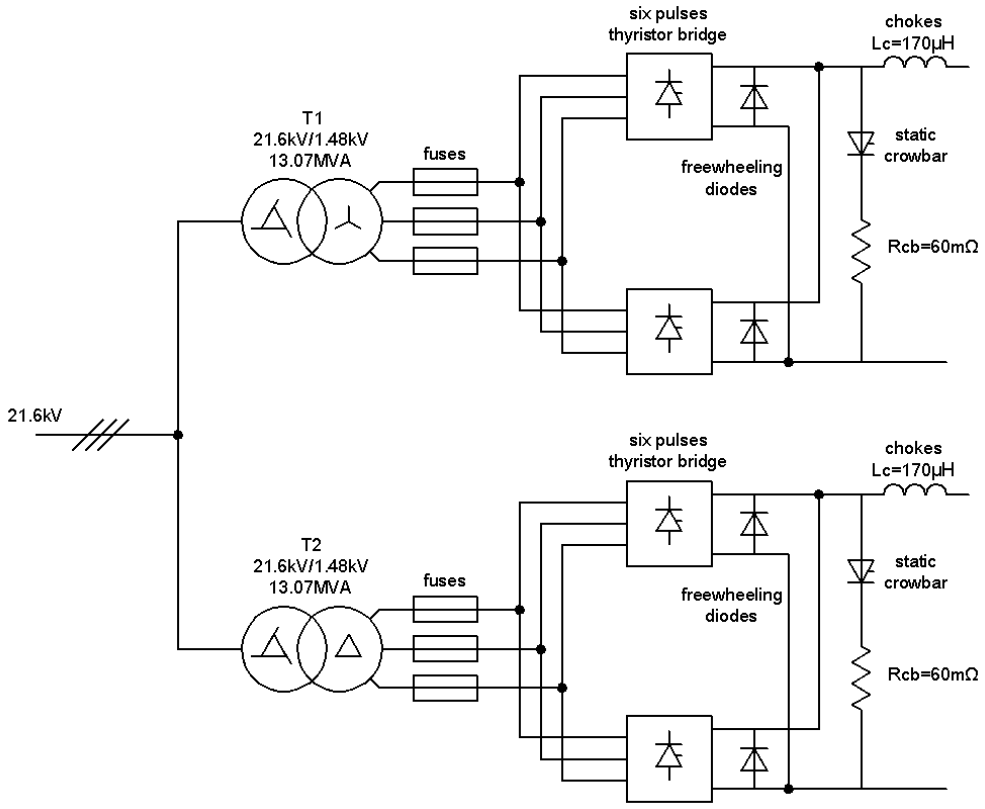

Figure 6 – “A unit” simplified electrical scheme

When the two sub units are connected in parallel or in series the “A unit” becomes a 12 pulses converter.

The tests on the ByPass Switch require high current, so the sub units have been connected in parallel: each “A unit” can supply a direct current of 16.248kA for 0.5s.

The number of “A units” needed for the tests depends on the maximum current which they have to supply (see paragraph 1.1):

$$Aunit\_number \geq \frac{51.4kA}{16.248kA} = 3.16 \Rightarrow 4$$

In the RFX-mod normal operation 4 A units are connected in parallel via a collector; thanks to the phase shift between the windings it is possible to obtain a 24 pulses ac/dc converter which can supply up to 65kA dc for 0.5ms.

The A unit which are connected in parallel are A05, A06, A07, A08.

2.1.2 Link between ac/dc converters and BPS

The BPS is linked to the 4 A units by mean of the cables of the RFX-mod plant, about 35m long.

The first part "cable 1" is from the converters to the collector near the switch PNSS, about 5m long; it is composed of aluminum busbars which form a rectangular loop (3.5mx1.5m) and of 0.5m long cable.

The resistance of "cable 1", at 20°C, is estimated to be:

$$R_{cable1} = 0.43m\Omega$$

Its parasitic inductance is estimated to be:

$$L_{cable1} = 7\mu H$$

The second part of the link, "cable 2" from the collector to the BPS, is composed of cables arranged as shown in Figure 7:

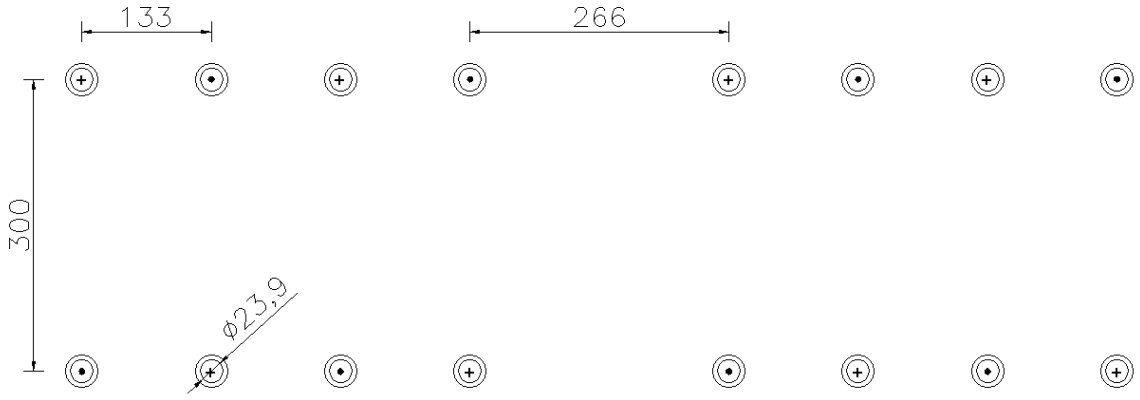

Figure 7 – Arrangement of the cables [mm]

The resistance of one cable is 1.3mΩ at 20°C, so the total resistance R_{cable2} is:

$$R_{cable2} = \frac{1.3}{4} \cdot 2 = 0.65m\Omega$$

The parasitic inductance has been estimated using FEMM:

$$L_{cable2} = 4.11\mu H$$

2.1.3 Busbars

The busbars from the BPS to the R_{eq} (identified with "cable 3" in Figure 4) have been designed to have parasitic inductance larger than that presently estimated by ASI for the QPC prototype around 3 μH; its value has been measured:

$$L_{cable3} = 3.77\mu H$$

While the resistance value (measured) of the busbars is:

$$R_{cable3} = 93\mu\Omega$$

2.2 Numerical simulations of the test circuit operation

A numerical simulation of the test circuit operation has been set up to verify the satisfaction of the required test condition and in particular the possible necessity of an inductance in series to the converters to reduce the current ripple. The PSIM model is shown in Figure 8.

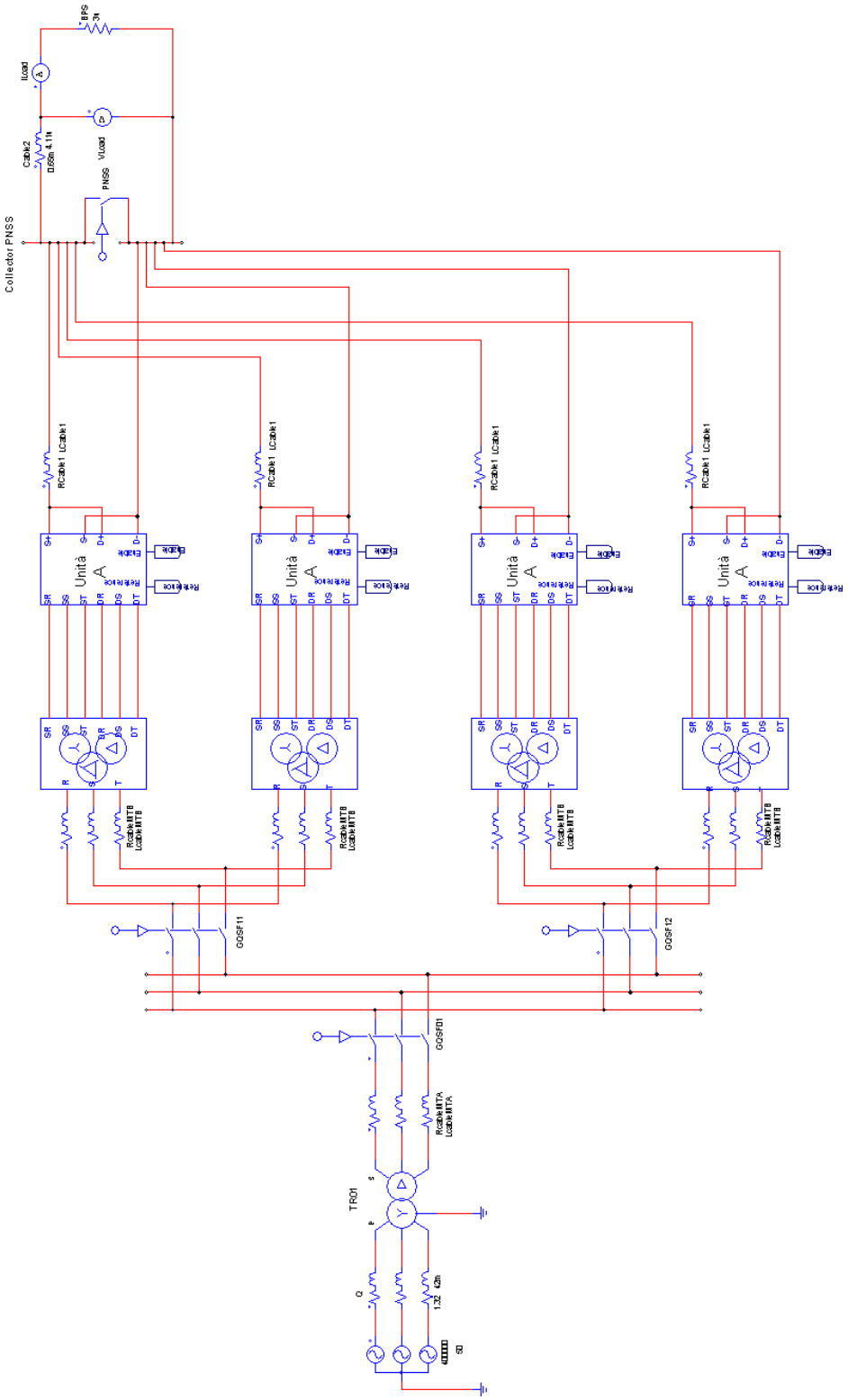

Figure 8 – PSIM Electrical model

2.2.1 Results of the numerical simulation

The converters output current is shown in Figure 9:

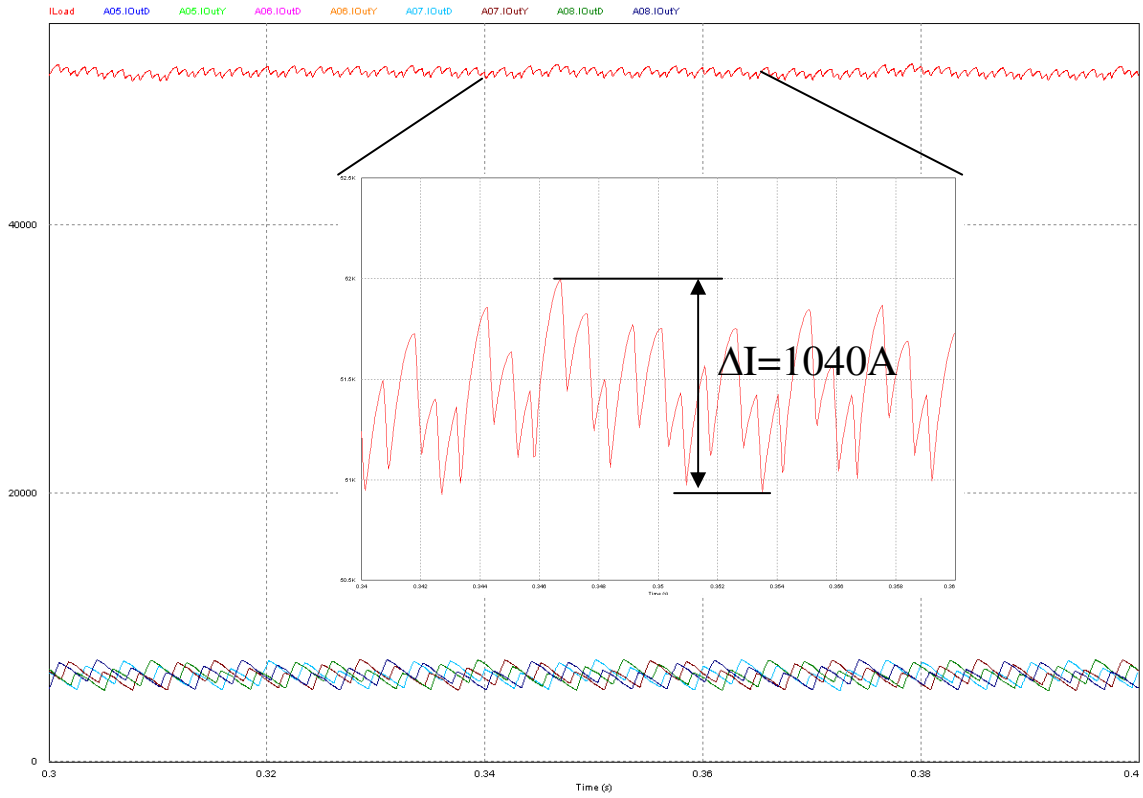

Figure 9 – Converters output current

The current ripple is:

$$Ripple = \frac{\Delta I}{I_{nom}} \cdot 100 = \frac{1040}{51400} \cdot 100 = 2.02\%$$

The ripple value is acceptable and so no series inductor is needed.

The circuit shown in Figure 8 has been used to assess also the current ripple at 25,7kA; in this case the current ripple is:

$$Ripple = \frac{\Delta I}{I_{nom}} \cdot 100 = \frac{810}{25700} \cdot 100 = 3.15\%$$

this value is still acceptable and no additional series inductor is required.

2.3 Measurements

The measurement points are shown in Figure 10:

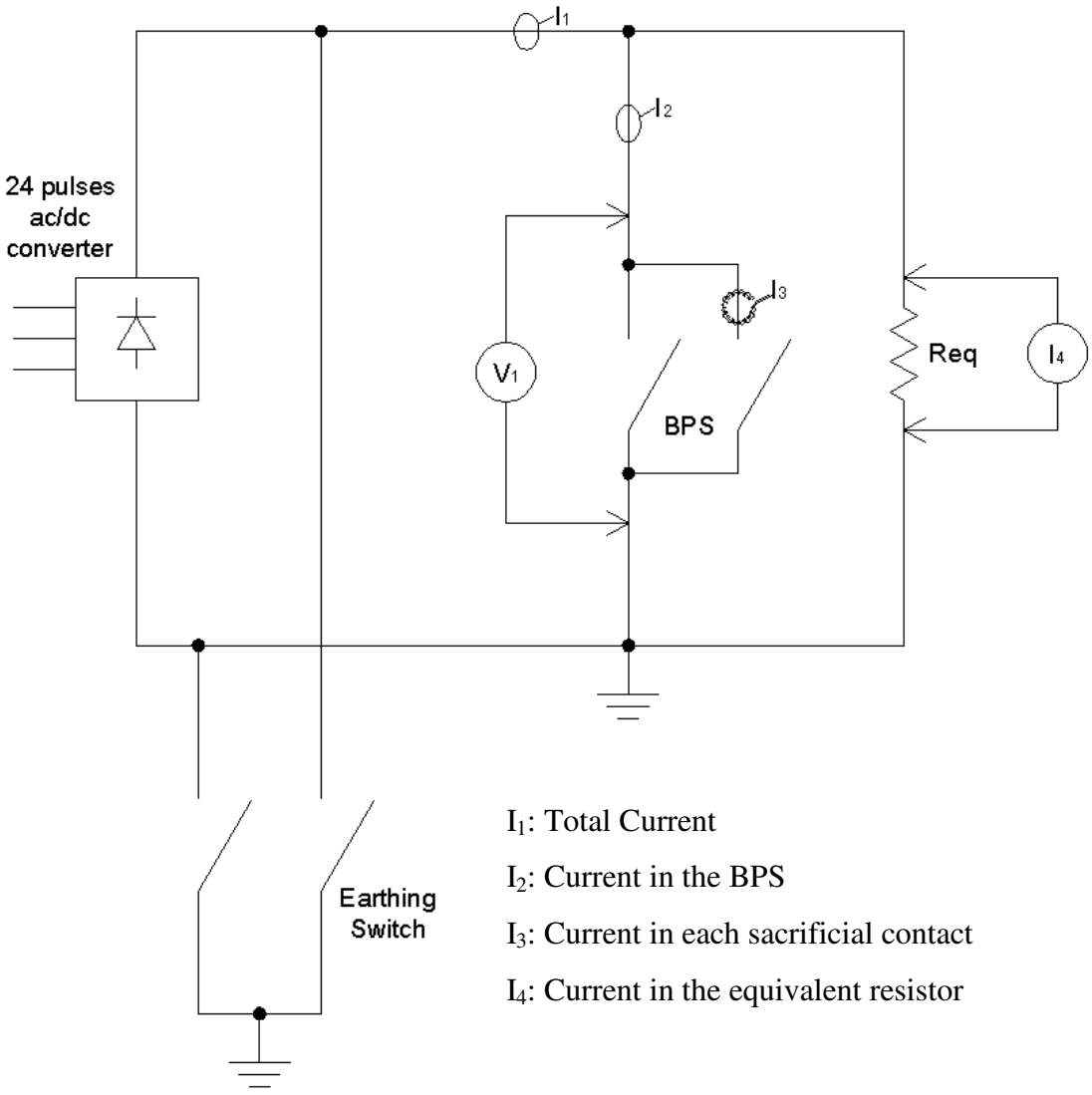

Figure 10 – Measurements

2.4 Control, protection and data acquisition systems

The general requirements for the tests on the BPS are:

- Remote Control System: to control the ByPass Switch and the ac/dc converters;
- Protection System: to stop the ac/dc converters in case of a failure;
- Data Acquisition System: to acquire and save the measurements from the field.

The control, protection and data acquisition system which has been set up is shown in Figure 11:

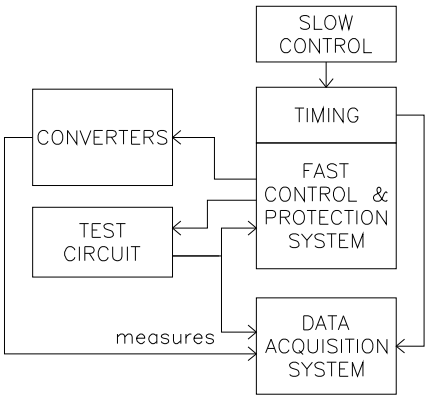

Figure 11 – Control, protection and data acquisition systems

The slow control is operated by a standard Siemens S7 PLC and consists in the following function:

- Collect status from and send slow commands to the test circuit;
- Send the parameters to the fast control system;
- Initiate the pulse sequence;
- Control the BPS outside pulse sequence.

The fast control and protection system is composed of a timing board and two klink (board developed at Consorzio RFX which implements FPGA) and perform the following functions:

- Coordinate the time sequence (start converters, open BPS, …);
- Collect status from and send slow commands to the test circuit;
- Collect measurements from the circuit in order to protect it;
- Stop the converters in case of fault.

2.4.1 List of signals

Digital signals

Table 3 – List of digital signals

id	*type*	*Fast*	*Slow*
EARTHING_SW_OPEN	STATUS		X
EARTHING_SW_CLOSED	STATUS		X
START_CONV	COMMAND	X	
STOP_CONV	COMMAND	X	
BPS_AUX_V	STATUS	X	X
BPS_PRESSURE	STATUS		X
BPS_OPEN	STATUS	X	X
BPS_CLOSED	STATUS	X	X
OPEN_BPS_KL	COMMAND	X	
OPEN_BPS_PLC	COMMAND		X
CLOSE_BPS	COMMAND		X
T_START_END	COMMAND	X	
T_OPEN_BPS	COMMAND	X	
T_ON_OFF_IGCT	COMMAND	X	
FAULT	STATUS	X	X
RESET	COMMAND		X
ENABLE_EXIT	COMMAND		X
START	COMMAND		X

Analog signals

Table 4 – List of analog signals

#	Description	id
1	Arc Votlage – Filtered	VARCF
2	Arc Votlage	VARC
3	Total Current – Filtered	ITOTF
4	Total Current	ITOT
5	Current on the ByPass Switch – Filtered	IBPSF
6	Current on the ByPass Switch	IBPS
7	Current on the Equivalent Resistor – Filtered	IREQF
11	Current on the Equivalent Resistor	IREQ
12	Contacts distance	DCON
13	A5 Unit – Sub Unit 1 – Output Voltage	A05BL05_UD01VA
14	A5 Unit – Sub Unit 2 – Output Voltage	A05BL05_UD02VA
15	A5 Unit – Sub Unit 1 – Output Current	A05BL05_ID01VA
16	A5 Unit – Sub Unit 2 – Output Current	A05BL05_ID02VA
17	A6 Unit – Sub Unit 1 – Output Voltage	A06BL06_UD01VA
18	A6 Unit – Sub Unit 2 – Output Voltage	A06BL06_UD02VA
19	A6 Unit – Sub Unit 1 – Output Current	A06BL06_ID01VA
20	A6 Unit – Sub Unit 2 – Output Current	A06BL06_ID02VA
21	A7 Unit – Sub Unit 1 – Output Voltage	A07BL07_UD01VA
22	A7 Unit – Sub Unit 2 – Output Voltage	A07BL07_UD02VA
23	A7 Unit – Sub Unit 1 – Output Current	A07BL07_ID01VA
24	A7 Unit – Sub Unit 2 – Output Current	A07BL07_ID02VA
25	A8 Unit – Sub Unit 1 – Output Voltage	A08BL08_UD01VA
26	A8 Unit – Sub Unit 2 – Output Voltage	A08BL08_UD02VA
27	A8 Unit – Sub Unit 1 – Output Current	A08BL08_ID01VA
28	A8 Unit – Sub Unit 2 – Output Current	A08BL08_ID02VA
29	Current on the sacrificial contact 1	ICS1
30	Current on the sacrificial contact 2	ICS2
31	Current on the sacrificial contact 3	ICS3
32	Current on the sacrificial contact 4	ICS4
33	Current on the sacrificial contact 5	ICS5
34	Current on the sacrificial contact 6	ICS6

2.5 Pictures of the Test Facility

The Test Facility has been setup according to the one described and presented in Figure 4 and in Figure 10.

The BPS has been installed in the R6 poloidal room as shown in Figure 12 and in Figure 13.

Figure 12 – R6 Poloidal room

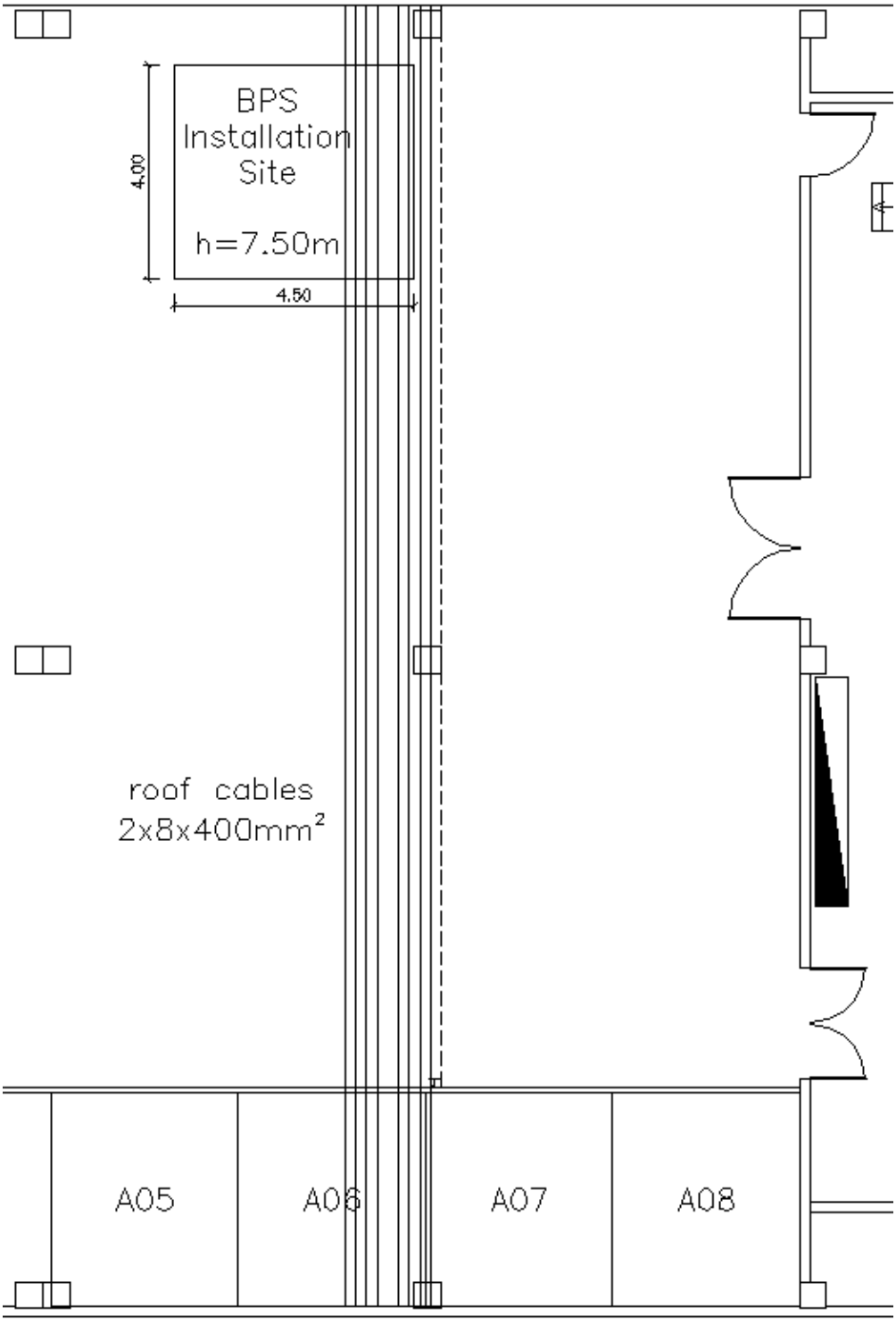

Figure 13 – R6 Poloidal room planimetry

In Figure 14 is shown a picture of the test circuit:

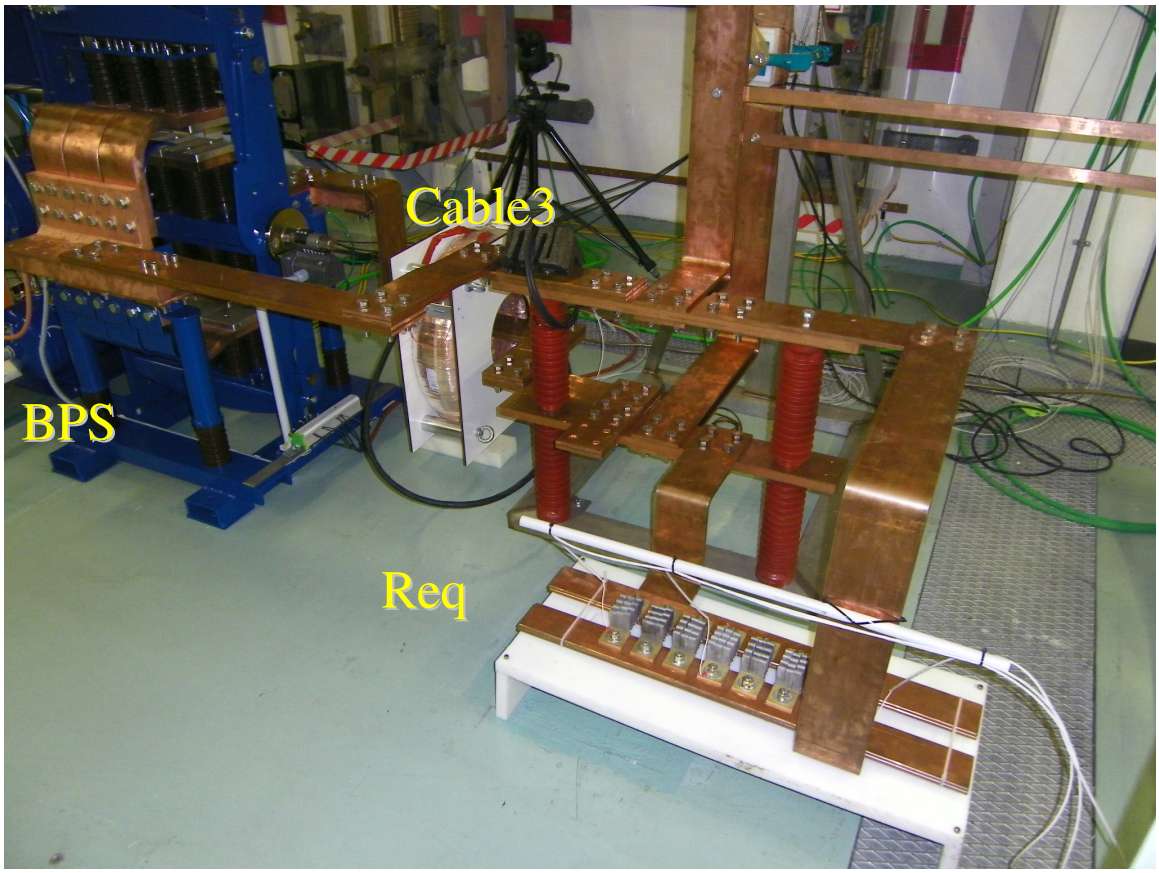

Figure 14 – Picture of the Test Circuit

Attachment 5

EXCERPT FROM CONSORZIO RFX INTERNAL NOTE: RFX_BA_TN_33: Descrizione del circuito di prova del prototipo di Quench Protection Circuit per JT-60SA per la valutazione del rischio elettromagnetico

1 Introduzione

Il Quench Protection Circuit per JT-60SA è composto da un interruttore bidirezionale in grado di aprire un circuito percorso da una corrente continua di a 25,7 kA con una tensione riapplicata di 4,2 kV e da un resistore di scarica.

Il suo scopo è di scaricare l'energia immagazzinata nei magneti superconduttori del tokamak JT-60SA, in costruzione in Giappone, in caso di quench (ovvero perdita delle caratteristiche superconduttive), commutando la corrente nel resistore di scarica.

Sono previste due tipologie diverse di QPC: una per il circuito poloidale e una per il circuito toroidale.

Il principio di funzionamento è schematizzato in Figura 1:

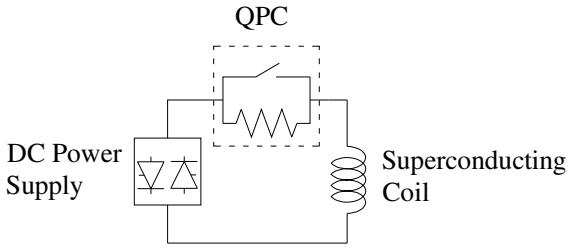

Figura 1 - Principio di funzionamento QPC

La particolarità dell'interruttore descritto è la sua abilità nell'interrompere una corrente senza bisogno di una counter pulse network e in pratica senza archi elettrici di energia elevata.

L'interruttore è costituito dal parallelo di un interruttore meccanico detto ByPass Switch e di un interruttore statico a IGCT detto Static Circuit Breaker e perciò è definito interruttore ibrido (Hybrid Circuit Breaker).

I test descritti in questa nota tecnica prevedono l'impiego degli impianti di RFX-mod presenti in sala R6 poloidale e in grado di fornire la corrente di prova. Non verrà utilizzato alcun induttore aggiuntivo, per cui lo schema semplificato della prova è riportato in Figura 2:

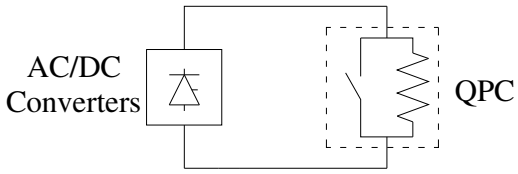

Figura 2 - Circuito di prova semplificato

2 Pianta R6

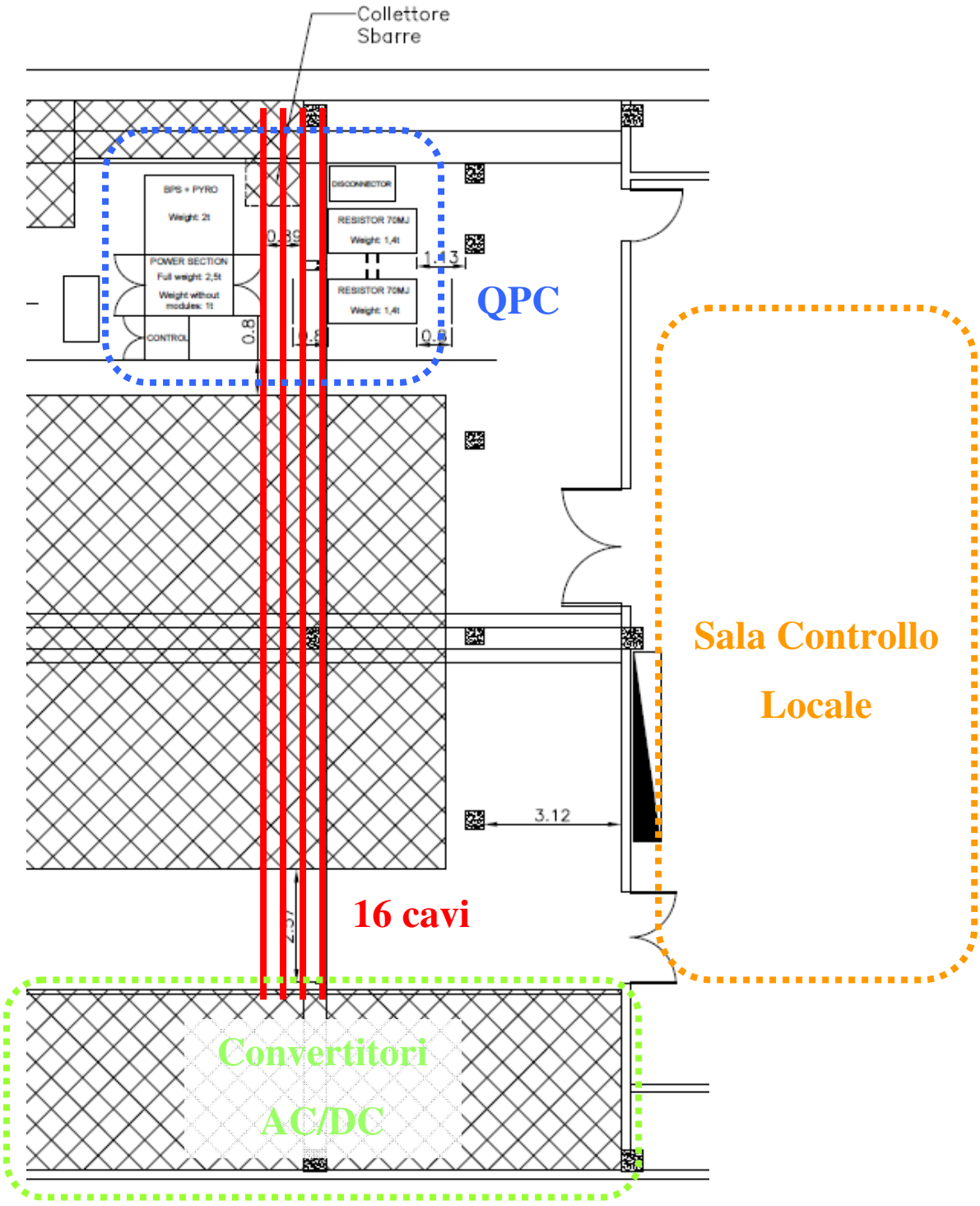

Figura 3 – Pianta luogo installazione

I 16 cavi di potenza che alimentano QPC fanno parte dell'impianto di alimentazione di RFX-mod e in particolare dell'avvolgimento magnetizzante. Essi sono posati su scalette in ferro ancorate al soffitto della sala poloidale e disposti come mostrato in Figura 4:

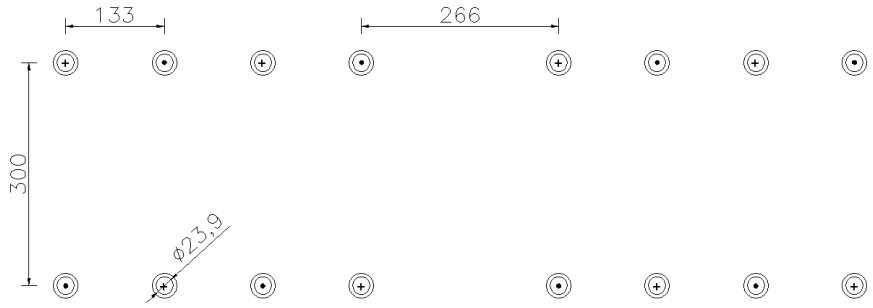

Figura 4 – Cavi di collegamento Convertitori – QPC (misure in [mm])

Si noti il collegamento atto a minimizzare l'induttanza parassita.

3 Forme d'onda previste

I test su QPC saranno di tipo impulsivo, ciascuno della durata massima di 500 ms con un dutycicle minimo di un impulso ogni 10 minuti.

Le forme d'onda previste per corrente e tensone del QPC poloidale sono riportate in Figura 5:

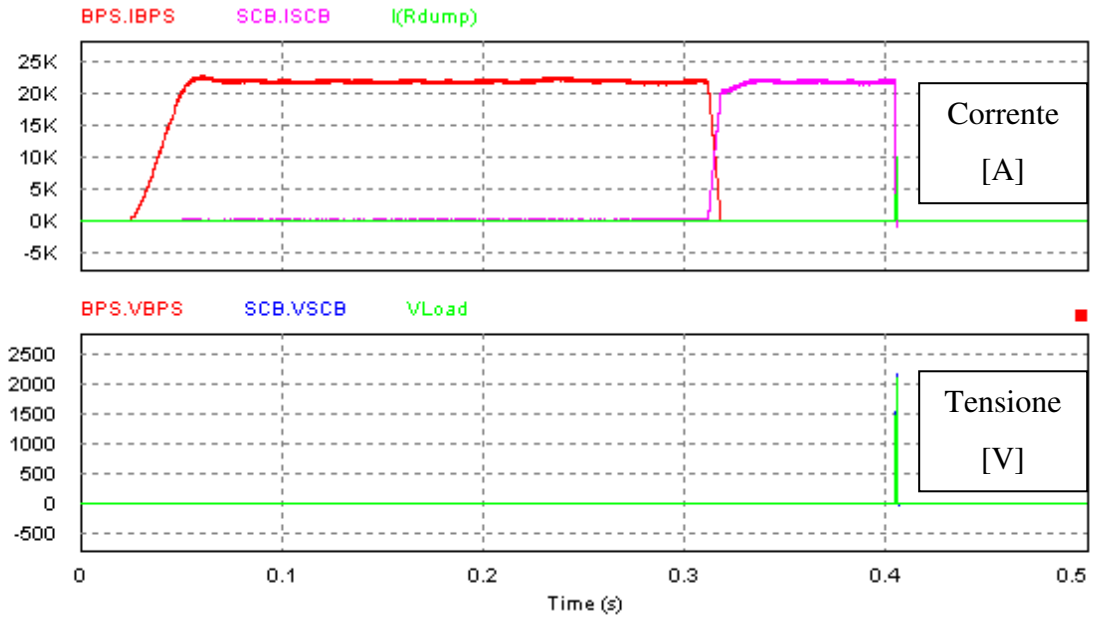

Figura 5 – Forme d'onda per QPC poloidale

Per quanto riguarda la forma d'onda di corrente si nota come la corrente scorra inizialmente sul ByPass Switch (BPS), poi venga commutata sull'interruttore statico (SCB) che quando apre la commuta (per un brevissimo periodo) sul resistore di dump.

La tensione rimane molto bassa (inferiore a 50 V) fino a quando non apre SCB, a quel punto la tensione risulta essere il prodotto tra la corrente e il valore della resistenza del resistore di dump.

Analogamente in Figura 6 sono riportate le forme d'onda previste per corrente e tensone per il QPC toroidale:

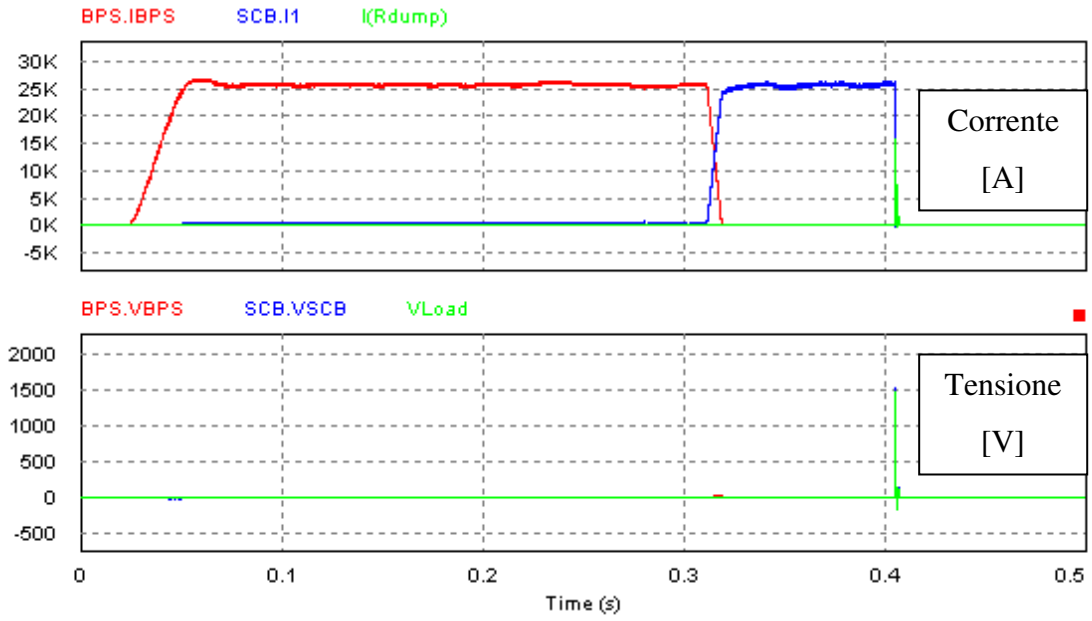

Figura 6 – Forme d'onda per QPC toroidale

Attachment 6

EXCERPT FROM CONSORZIO RFX INTERNAL NOTE: RFX_BA_TN_20: JT-60SA TFC PS Short Circuit Currents

This document aims to estimate the short circuit currents in the case of a fault at the connection point between the ac cables and the thyristor bridge of the TFC converters.

1 Electrical Network

Figure 15 [1] shows the electrical network of the JT-60SA TFC PS and the fault point which will be analyzed:

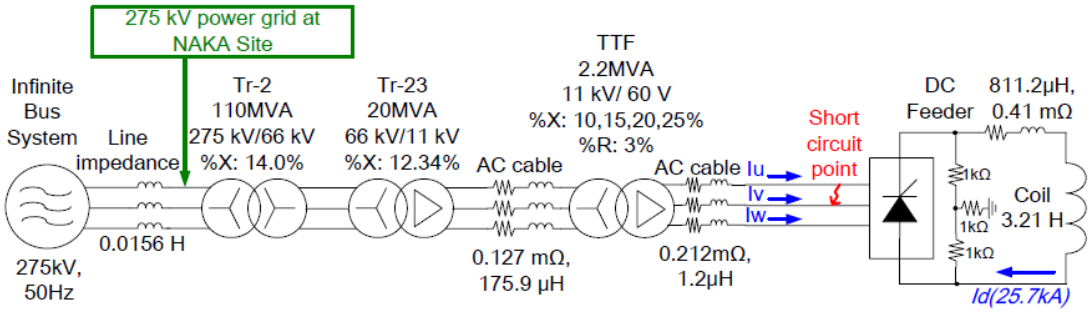

Figure 15 - Electrical Network of the TFC PS

2 Initial calculations

At first we can consider a three phases short circuit at the highlighted point, without any load connected (so we can neglect the converter after the short circuit). This assumption is a conservative point of view, because the peak current depends also on the difference between the short circuit current and the previous absorbed current.

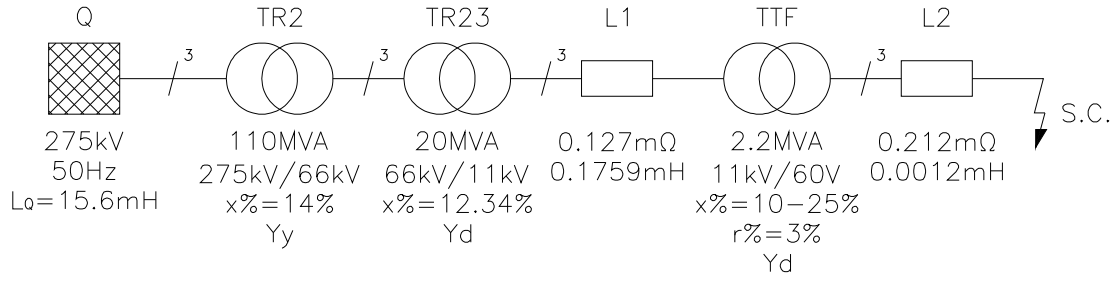

Figure 16 - Electrical scheme

It is possible to calculate the parameters of the network as shown in the following steps.

We can assume that the 0.0156H Line impedance (Figure 15) is the impedance of the network at NAKA site.

2.1 Q – power grid at NAKA Site

The inductive reactance X_Q is:

$$X_Q = 2 \cdot \pi \cdot f \cdot L_Q \approx 314 \cdot 15.6 = 4898.4\ m\Omega$$

2.2 TR2

The nominal impedance Z_{nTR2} of the transformer TR2 is:

$$Z_{nTR2} = (U1n)^2 / Sn = (275000)^2 / (110 \cdot 10^6) = 687.5\ \Omega$$

The inductive reactance X_{TR2} is:

$$X_{TR2} = x\% \cdot Z_{nTR2} = 0.14 \cdot 687.5 = 96.25\ \Omega$$

2.3 TR23

The nominal impedance Z_{nTR23} of the transformer TR23 is:

$$Z_{nTR23} = (U1n)^2 / Sn = (66000)^2 / (20 \cdot 10^6) = 217.8\ \Omega$$

The inductive reactance X_{TR23} is:

$$X_{TR23} = x\% \cdot Z_{nTR23} = 0.1234 \cdot 217.8 \approx 26.877\ \Omega$$

2.4 L1

The inductive reactance X_{L1} of the L1 impedance is:

$$X_{L1} = 2 \cdot \pi \cdot f \cdot L_{L1} \approx 314 \cdot 0.1759 = 55.2326\ m\Omega$$

2.5 TTF

The nominal impedance Z_{nTTF} of the transformer TTF is:

$$Z_{nTTF} = (U1n)^2 / Sn = (11000)^2 / (2.2 \cdot 10^6) = 55\ \Omega$$

The resistance R_{TTF} is:

$$R_{TTF} = r\% \cdot Z_{nTTF} = 0.03 \cdot 55 = 1.65\Omega$$

The inductive reactance X_{TTF}, assuming x%=10, is:

$$X_{TTF} = x\% \cdot Z_{nTTF} = 0.10 \cdot 55 = 5.5\Omega$$

2.6 L2

L2 it is assumed to be a 10m cable with L_{L2}=0.12 mH/km, R_{L2}=0.0212 Ω/km, as described in [1].

The inductive reactance X_{L2} of the L2 impedance is:

$$X_{L2} = 2 \cdot \pi \cdot f \cdot L_{L2} \approx 314 \cdot 0.0012 = 0.3768 \text{ m}\Omega$$

2.7 Summary of the impedances values

It can be used the "per unit method", referring all the impedance values to the TTF secondary voltage value Ub. Each impedance has to be referred to Ub= 60V, with the following equation:

$$Z_b = Z_a \cdot (U_b / U_a)^2$$

Where Ua is the rated voltage of each element, or in the case of the transformers Ua is their primary rated voltage.

The resulting values are listed in the following table:

	Q	TR2	TR23	L1	TTF	L2
R [mΩ]	0	0	0	3.78E-06	0.04909	0.212
X [mΩ]	2.33E-04	4.58E-03	2.22E-02	1.64E-03	0.16364	0.3768

Table 2-1

The total impedance is composed of:

R_{tot} = (3.78 E-6 + 0.04909 + 0.212) ≈ 0.2611 mΩ

X_{tot} = (2.33 E-4 + 4.58E-3 + 2.22E-2 + 1.64E-3 + 0.16364 + 0.3768) ≈ 0.5691 mΩ

$Z_{tot} = (R_{tot}^2 + X_{tot}^2)^{0.5} = 0.6261$ mΩ

3 Fault analysis

In the following paragraphs some fault conditions will be considered. The analysis will follow the requirements of the standard IEC EN 60909-0 and there will be some concepts taken from "Lezioni di Impianti Elettrici" by A. Paolucci [2].

The analysis of the short circuit currents foresees the estimation of two values of current: the maximum and the minimum which may occur at a network node. To assess them, the

standard introduces a “voltage factor” which multiplies the voltage value at the considered node. The recommended “voltage factor” values are listed in [3] for different voltage classes. The aim of this document is to assess the maximum value of the SC currents. Therefore it will be used 1 as “voltage factor”, which is the value for the maximum short circuit current calculation at low voltages (IEC EN 60909-0).

3.1 Three-Phase Short Circuit

This is a symmetric fault and so it is possible to use the equivalent single phase circuit, as shown in the following pictures:

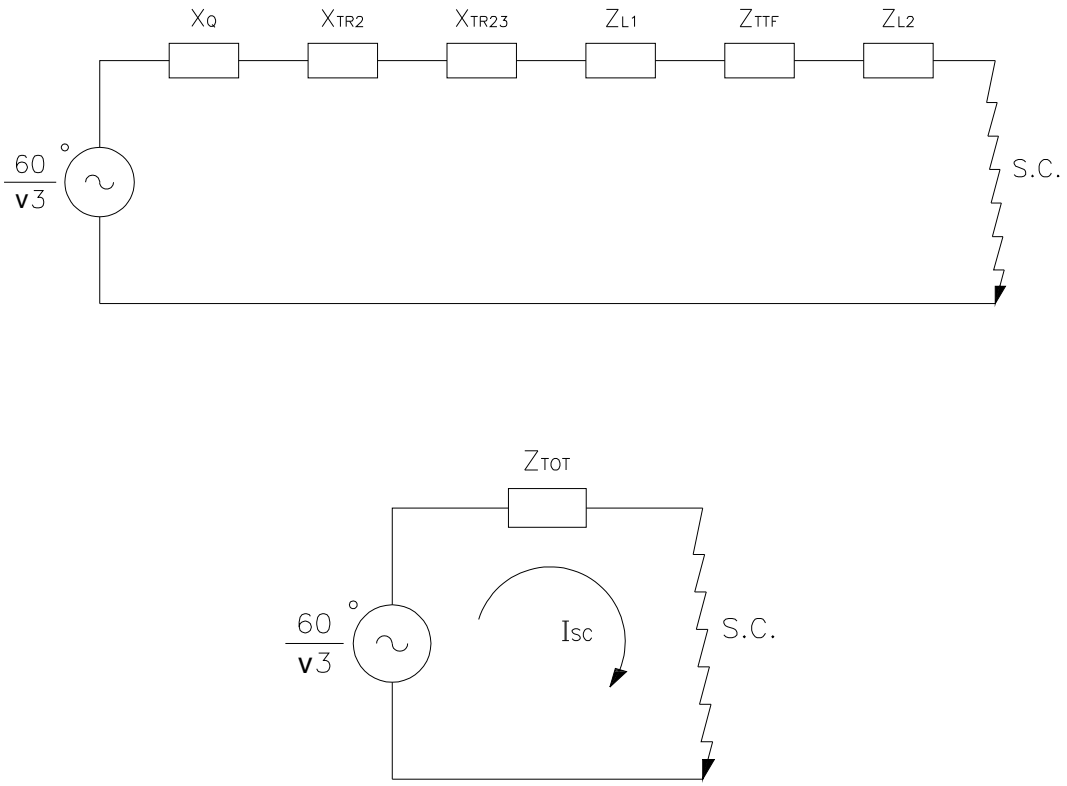

Figure 17 – Equivalent single phase circuit

The short circuit current Isc (steady state r.m.s.) is:

$$I_{sc} = \frac{U}{\sqrt{3} \cdot Z_{TOT}} = \frac{60}{\sqrt{3} \cdot 0.6261} \approx 55kA$$

The peak current can be computed following the equation (IEC EN 60909-0):

$$I_{Peak} = \sqrt{2} \cdot \chi \cdot I_{sc}$$

Where χ is calculated as:

$$\chi = 1.02 + 0.98 \cdot e^{-3\frac{R_{TOT}}{X_{TOT}}} = 1.2674$$

The peak current is then:

$$I_{peak} = \sqrt{2} \cdot 1.2674 \cdot 55000 \approx 98.6kA$$

In principle this kind of fault has a very low probability to occur during normal operation, but it can occur as a consequence of incorrect maintenance operations.

3.2 Phase-to-Phase Short Circuit

The following picture shows the three-phase circuit with the short circuit in between phase 2 and phase 3: The fault current flows in these two phases, while in phase 1 the fault current is null.

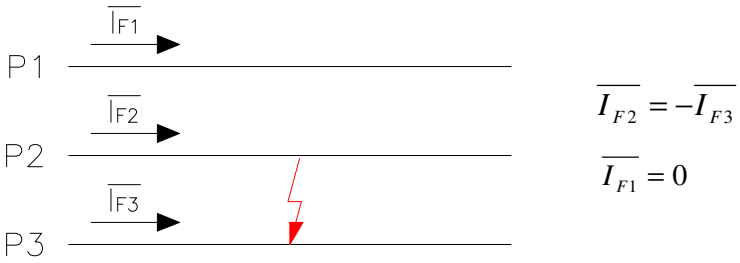

Figure 18 – Phase 2 to phase 3 short circuit

In this case the system is not any more symmetric and so we have to use the method of "symmetrical components" [2],[3].

In particular this fault uses only the positive sequence elements and the negative sequence elements: there are only transformers and lines in the network, and so it is possible to assume that the negative sequence elements are equal to the positive sequence elements.

The positive sequence impedances are the same used in the analysis of the three-phase short circuit.

We can assume that the negative sequence impressed voltages are negligible, so the electrical scheme of the resulting symmetrical components is:

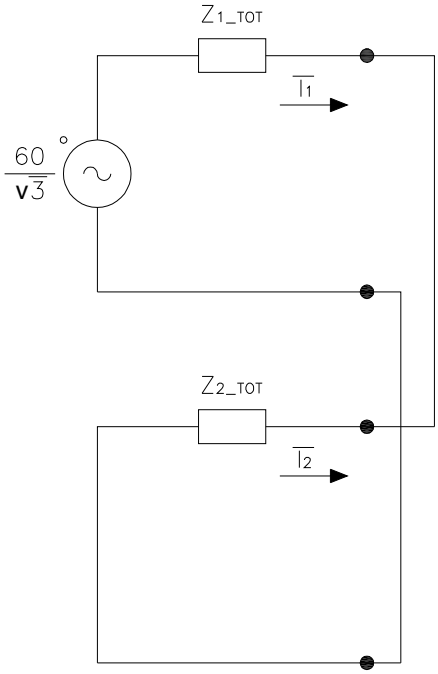

Notation:

1 - Positive sequence element/current

$$\overline{I_2} = -\overline{I_1}$$

Figure 19 – Symmetrical Sequences involved in the phase-to-phase short circuit

$Z_{1\_TOT} = 0.2611 + j\,0.5691\ m\Omega$

$Z_{2\_TOT} = 0.2611 + j\,0.5691\ m\Omega$

The positive sequence current is:

$$\overline{I_1} = \frac{60}{\sqrt{3}} \cdot \frac{1}{Z_{1\_TOT} + Z_{2\_TOT}}$$

$$\overline{I_1} = \frac{60}{\sqrt{3}} \cdot \frac{1}{2 \cdot (0.2611 + j0.5691)} = 1.1535 - j2.5143 = 27.66 \cdot e^{j-65.35} kA$$

The negative sequence current is:

$$\overline{I_2} = -\overline{I_1} = -1.1535 + j2.5143 kA$$

The fault currents are:

$$\overline{I_{F2}} = \alpha^2 \cdot \overline{I_1} + \alpha \cdot \overline{I_2} = (\alpha^2 - \alpha) \cdot \overline{I_1} = \sqrt{3} \cdot e^{-j90} \cdot \overline{I_1}$$

$$\overline{I_{F3}} = -\overline{I_{F2}}$$

With

$\alpha = e^{j120}$

The absolute value is:

$$I_{F2} = I_{F3} = I_1 \cdot \sqrt{3} = 27.66 \cdot \sqrt{3} = 47.91kA$$

The peak value can be calculated as:

$$I_{F2\_Peak} = \sqrt{2} \cdot \chi \cdot I_{F2}$$

χ is the same calculated in section 3.1, as the standard recommends (it is justified also because the R/X value is the same), so:

$$I_{F2\_Peak} = \sqrt{2} \cdot 1.2674 \cdot 47.9 = 85.9kA$$

3.3 Phase-to-Earth Short Circuit

The following picture shows the three-phase circuit with the short circuit between phase 1 and earth: The fault current flows only in phase 1, while in the other two phases the fault current is null.

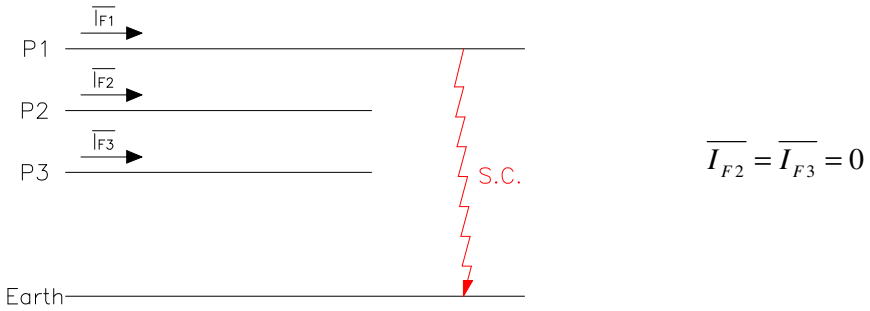

Figure 20 – Phase 1 to Earth fault

This kind of fault is not symmetric and so we have to consider the "symmetrical component method". The equivalent scheme is composed of the positive sequence, the negative sequence and the zero sequence circuits, connected in series (IEC EN 60909-0).

The positive and the negative sequences are the same of the previous paragraph, while for the zero sequence impedance we evaluate the possibility of having a zero sequence current flowing through the elements of the network.

Figure 21 shows the theoretical circuit to measure the zero sequence impedance, applying a zero sequence voltage generator.

We assume that the ground is equipotential, and so there are not voltage drops in the return circuit.

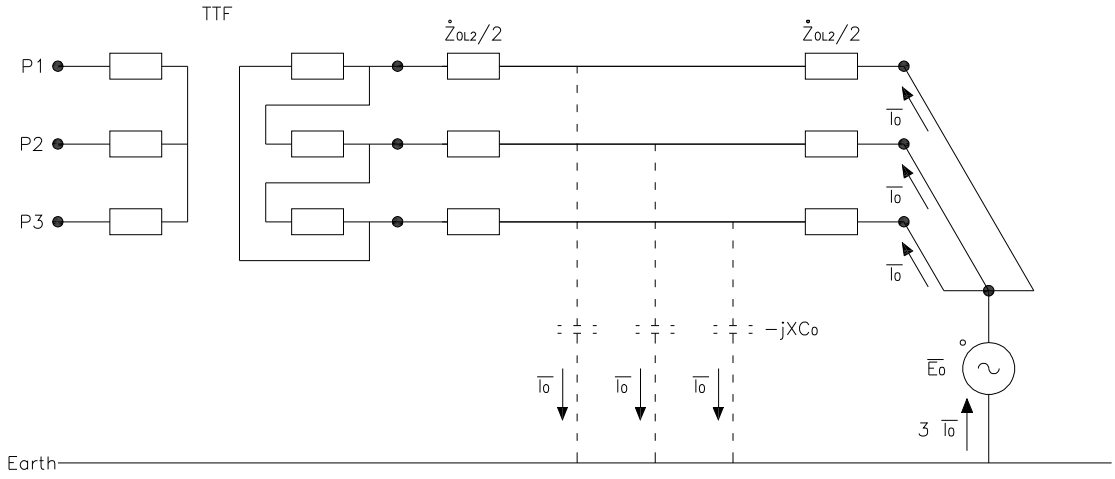

Figure 21 – Zero sequence impedance estimation

The longitudinal impedance Z_{L2} assumes a different value (indicated as Z_{0L2}) for the zero sequence due to the different fluxes produced by the zero sequence currents.

We can use the T equivalent-circuit model for the cable L2, where the Z_{0L2} is split in two equal parts, and the central branch is the earth capacity (and so the capacity between the main conductor and the screen) of the cable.

If we consider the TTF connection, we can see that there is not possibility for the zero sequence current to pass through. The only way to close the loop for the zero sequence current is to pass through the earth capacity C_0 of the ac cable L2.

It is necessary to estimate the C_0 value.

It would be possible to assess C_0 using the equation:

$$C_0 = \frac{2 \cdot \pi \cdot \varepsilon_0 \cdot \varepsilon_r}{\ln\left(\frac{ds}{dc}\right)}$$

Which is the capacitance of a coaxial cable (per length unit), where ds is the diameter of the screen and dc is the diameter of the conductor, but they are not yet known.

Assuming a C_0 value of 1μF (which is very high compared to a possible actual value) the capacitive reactance XC_0 is:

$$XC_0 = \frac{1}{\omega \cdot C_0} = \frac{1}{2 \cdot \pi \cdot 50 \cdot 10^{-6}} \approx 3185\Omega$$

As aforementioned the longitudinal impedance assumes bigger values in the case of zero sequence than in the case of positive (and negative) sequences, generally $Z_{0L}/Z_L \approx 3$.
So it is possible to further simplify the circuit because Z_{0L2} (~Ω) is negligible compared to XC_0 (~kΩ) which is certainly underestimated.

The resulting zero sequence scheme is presented in Figure 22:

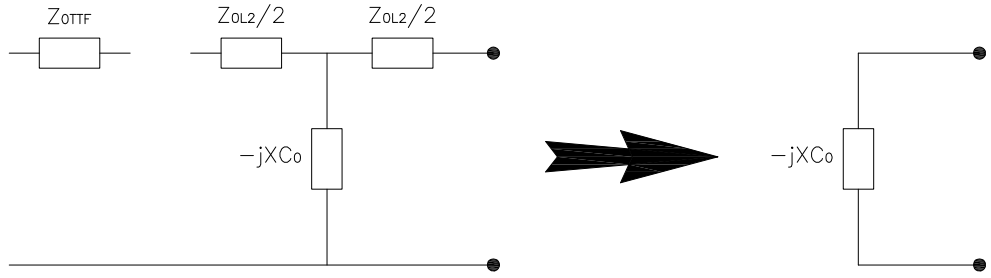

Figure 22 – Zero sequence impedance assumption

All the components located upstream of the TTF is irrelevant from the point of view of the zero sequence because of the connection of the secondary of this transformer.

The resulting symmetric component circuit is shown in Figure 23:

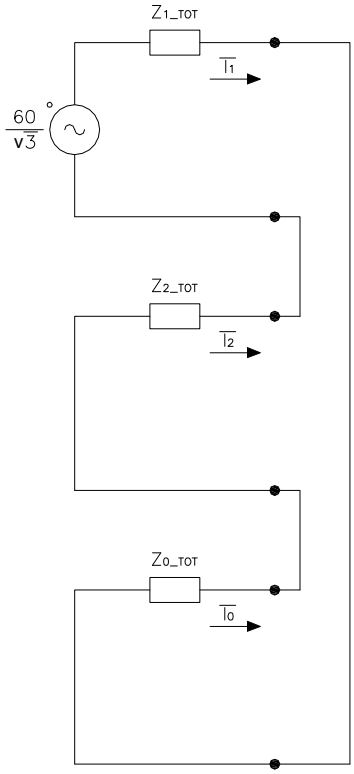

$$\overline{I_1} = \overline{I_2} = \overline{I_0}$$

$$\overline{I_{F1}} = \overline{I_1} + \overline{I_2} + \overline{I_0} = 3 \cdot \overline{I_1}$$

Figure 23 - Symmetrical Sequences involved in the phase-to-earth short circuit

The resulting fault current can be calculated as:

$$\overline{I_{F1}} = 3 \cdot \frac{60}{\sqrt{3}} \cdot \frac{1}{\overset{\circ}{Z}_{1\_TOT} + \overset{\circ}{Z}_{2\_TOT} + \overset{\circ}{Z}_{0\_TOT}} \approx 3 \cdot \frac{60}{\sqrt{3}} \cdot \frac{1}{-jXC_0} = j \cdot \frac{\sqrt{3} \cdot 60}{3185} \approx 33mA$$

The peak current can be at most twice (depending on the fault time and χ value) and it is still a negligible value compared to the other fault currents.

An alternative way to estimate the short circuit current is using the following equation [2],[4]:

$$Isc_{[A]} = \left[0.003 \cdot l\_ac_{[km]} + 0.2 \cdot l\_c_{[km]}\right] \cdot V_{[kV]}$$

Where:

- Isc is the fault current in case of phase-to-earth short circuit
- l_ac is the length of the aerial cable lines electrically connected to the analyzed point;
- l_c is the length of the cables electrically connected to the analyzed point;
- V is the voltage of the line.

In our case the short circuit current is:

$$Isc = 0.2 \cdot 0.01 \cdot 0.06 = 0.12mA$$

Which corresponds to a C_0 value of about 10nF and it confirms that the previous assumption of 1μF is very overestimated.
We can see that the fault current is negligible compared to the other analyzed cases, so it is possible to assume as infinite the impedance value of Z_0.

From the point of view of the voltage that the insulators have to withstand in this kind of fault, there are not insulation problems thanks to the very low voltage at the secondary side of the TTF transformer: If a phase is short-circuited to ground, the other phases reach a voltage-to-ground which is $\sqrt{3}$ times grater, but still not critical.

3.4 Phase-to-Phase-to-Earth Short Circuit

The scheme of Figure 24 shows the three-phase circuit with the short circuit which affects phase 2, phase 3 and earth: The fault current flows only in this two phases, while in phase 1 the fault current is null.

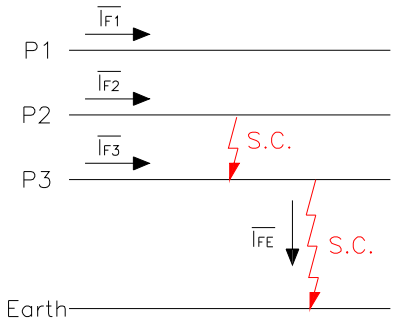

$$\overline{I_{FE}} = \overline{I_{F2}} + \overline{I_{F3}}$$

$$\overline{I_{F1}} = 0$$

Figure 24 – Phase 2 to Phase 3 to earth short circuit

Under the same assumptions considered in section 3.3, the resulting symmetrical component circuit (IEC EN 60909-0) is shown in the following picture:

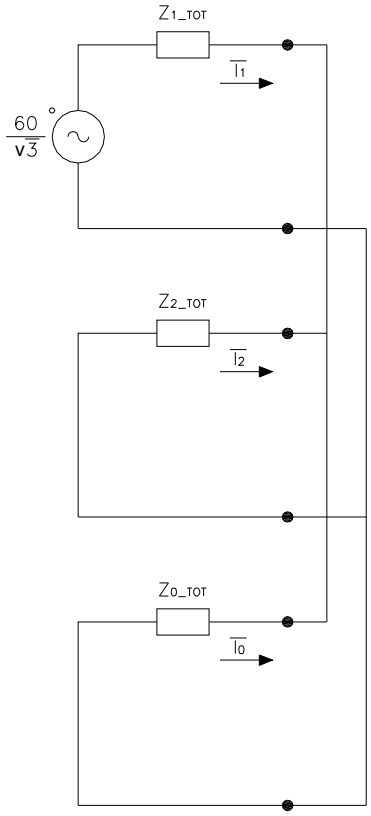

$$\overline{I_1} = \frac{60}{\sqrt{3}} \cdot \frac{\overset{\circ}{Z}_{2\_TOT} + \overset{\circ}{Z}_{0\_TOT}}{\overset{\circ}{Z}_{1\_TOT} \cdot \overset{\circ}{Z}_{2\_TOT} + \overset{\circ}{Z}_{1\_TOT} \cdot \overset{\circ}{Z}_{0\_TOT} + \overset{\circ}{Z}_{2\_TOT} \cdot \overset{\circ}{Z}_{0\_TOT}}$$

$$\overline{I_2} = -\frac{60}{\sqrt{3}} \cdot \frac{\overset{\circ}{Z}_{0\_TOT}}{\overset{\circ}{Z}_{1\_TOT} \cdot \overset{\circ}{Z}_{2\_TOT} + \overset{\circ}{Z}_{1\_TOT} \cdot \overset{\circ}{Z}_{0\_TOT} + \overset{\circ}{Z}_{2\_TOT} \cdot \overset{\circ}{Z}_{0\_TOT}}$$

$$\overline{I_0} = -\frac{60}{\sqrt{3}} \cdot \frac{\overset{\circ}{Z}_{2\_TOT}}{\overset{\circ}{Z}_{1\_TOT} \cdot \overset{\circ}{Z}_{2\_TOT} + \overset{\circ}{Z}_{1\_TOT} \cdot \overset{\circ}{Z}_{0\_TOT} + \overset{\circ}{Z}_{2\_TOT} \cdot \overset{\circ}{Z}_{0\_TOT}}$$

$$\overset{\circ}{Z}_{0\_TOT} \longrightarrow \infty$$

Figure 25 - Symmetrical Sequences involved in the phase-to-phase-to-earth short circuit

As can be easily seen the resulting fault currents are:

- $I_{F2}=I_{F3}$ with the same value calculated in section 3.2;
- $I_{FE} = 0$, for the same reasons seen in section 3.3.

4 Results summary

In Table 4-1 the fault currents in case of three-phase short circuit and phase-to-phase short circuit are listed, as a function of the inductive reactance x% of the TTF transformer.

x%	$Z_1=Z_2$	Three Phases Short Circuit		Phases-to-Phase Short Circuit	
	[mΩ]	Isc rms [kA]	Isc peak [kA]	Isc rms [kA]	Isc peak [kA]
10	0.626	55.3	99.2	47.9	85.9
15	0.702	49.4	91.8	42.8	79.5
20	0.778	44.5	85.4	38.6	74.0
25	0.856	40.5	79.9	35.1	69.1

Table 4-1 – Results summary

These values are computed in the same way as shown in section 3.

Increasing the inductive reactance x% from 10 to 25% the rms values of the short circuit currents are reduced of about 27%, while the peak values are reduced of about 20%.

The short circuit currents to ground are not listed because their values are negligible, thanks to the transformer connections.

5 Conclusions

The short circuit currents are very huge and they are listed in Table 4-1, the faults to ground are not critical issues, thanks to the transformer connections which do not allow their flow.

6 References

[1] Katsuhiro Shimada, “Preliminary analyses of short-circuit current at connection point of CS2, CS3, FPPC, and TFC PS converter” - JT60SA-PS-000162-1;

[2] Antonio Paolucci, “Lezioni di Impianti Elettrici”, CLEUP, ISBN 88-7178-632-7;

[3] IEC EN 60909-0:2001, “Short-circuit currents in three-phase a.c. systems”;

[4] CENELEC HD 637 S1:1999, “Power installations exceeding 1 kV a.c.”